

# **A STUDY OF TURBULENT FLOW OVER A BACKWARD FACING STEP**

A dissertation submitted in partial fulfillment of the requirements for the award of the degree  
of  
Master of Philosophy  
in  
Mathematics

by  
Sajid Ahmed  
Roll No.: 0412093001P, Registration No.: 0412093001  
Session: April, 2012  
Department of Mathematics  
Bangladesh University of Engineering and Technology  
Dhaka-1000, Bangladesh

Supervised by  
Dr. Md. Abdul Maleque  
Professor  
Department of Mathematics  
Bangladesh University of Engineering and Technology




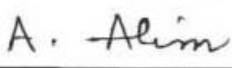
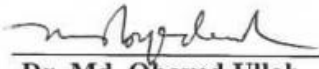
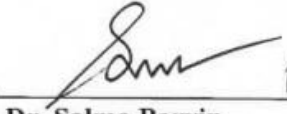

Department of Mathematics  
Bangladesh University of Engineering and Technology  
Dhaka-1000, Bangladesh  
March, 2017

The Thesis entitled  
**A STUDY OF TURBULENT FLOW OVER A BACKWARD  
FACING STEP**

Submitted by  
Sajid Ahmed

Roll no.: 0412093001P, Registration No.: 0412093001, Session: April, 2012  
has been accepted as satisfactory in partial fulfillment of the requirements for the award of the degree of  
**Master of Philosophy in Mathematics**  
on 18th March, 2017.

**Board of Examiners**


1.   
**Dr. Md. Abdul Maleque (Supervisor)** Chairman  
Professor  
Department of Mathematics  
BUET, Dhaka-1000
2.   
**Head** Member  
Department of Mathematics (Ex-Officio)  
BUET, Dhaka-1000
3.   
**Dr. Md. Obayed Ullah** 18.3.17 Member  
Professor  
Department of Mathematics  
BUET, Dhaka-1000
4.   
**Dr. Salma Parvin** 18.03.17 Member  
Associate Professor  
Department of Mathematics  
BUET, Dhaka-1000
5.   
**Dr. Md. Mustafa Kamal Chowdhury** 18.3.17 Member  
Ex-Professor (External)  
Department of Mathematics  
BUET, Dhaka-1000

## **Author's declaration**

I declare that the work in this dissertation has been carried out in accordance with the Regulation of Bangladesh University of Engineering and Technology, Dhaka-1000, Bangladesh. The work is original except where indicated by special references in the text and no part of it has been submitted for any other degree.

The dissertation has not been presented to any other university for examination either in Bangladesh or overseas.

Name: Sajid Ahmed

Signature: 

Date: 18-3-17

**Dedicated**

**to**

**My respected parents,**

**My beloved son and wife.**

## **Acknowledgements**

At first all praise go to Allah the Almighty who has kindly given the strength, wisdom and rahmah to do this job. Alhamdullillah. Secondly, I am grateful to my parents for their endless efforts and hard work for my wellbeing and success.

I am very much thankful to my thesis supervisor Professor Dr. Md. Abdul Maleque for his all-out support and help towards the completion of this thesis. He has encouraged me all the time since he took over the supervision of this thesis work. I owe him for his good guidance, constant inspiration and valuable suggestions. I am also grateful to Professor Dr. Md. Mustafa Kamal Chowdhury for agreeing to supervise my thesis unto his retirement. I thank Dr. Salma Parvin for extensively guiding me at various stages of this thesis work. I also thank Professor Dr. Md. Obayed Ullah for supporting me and providing me with some important books.

I am thankful to all the teachers of the Department of Mathematics, BUET including the Head for encouragements and supports all the time. At this scope I also thank the office staff of the Math Department, BUET.

I am grateful to the BUET authorities for providing me with all the infrastructural, internet and other necessary facilities.

## **Abstract**

Turbulence is the chaotic motion of fluid occurring in most of the natural and other flow fields. Since it is very difficult to treat the turbulent flow analytically, various techniques and models have been developed to describe turbulent flow - with the help of the increasing power of computers- numerically. The present study incorporates a numerical treatment of a turbulent flow over a backward facing step having a circular obstacle. The standard  $k-\varepsilon$  turbulence model is used to simulate and obtain the numerical results. This turbulence model has been solved using Galerkin weighted residual finite element method. The effect of size and position of the circular obstacle on the streamlines, velocity magnitude, pressure distribution, velocity profiles and turbulent kinetic energy profiles are presented graphically. The result shows that size and position of the obstacle has noteworthy effect on the aforementioned parameter profiles.

# Contents

Board of Examiners

Author's declaration

Acknowledgements

Abstract

Contents

Nomenclature

List of tables

List of figures

Page

## 1. Introduction

1.1 Basic Concepts: Laminar and Turbulent Flows	13
1.2 General Properties of Turbulence	14
1.3 Examples of Turbulence	18
1.4 Describing the Turbulent Flow	21
1.5 $k - \epsilon$ Turbulence Model	25
1.6 Backward Facing Step	26
1.7 Historical Background and Literature Review	27
1.8 Motivation	31
1.9 Objectives	32

## 2. Formulation

2.1 Problem formulation	33
2.2 Mathematical model	34
2.3 Boundary conditions	36
2.4 Wall functions	37

3. Methodology	
3.1 Numerical scheme	39
3.2 Meshes	41
3.3 Grid independence test	42
4. Results and Discussions	
4.1 Variation of the Size of the Obstacle	43
4.2 Variation of the Position of the Obstacle	42
5. Conclusion	
5.1 Conclusions from the Present Study	56
5.2 Suggestions for Further Study	57
References	58



## Nomenclature

<b>Symbol</b>	<b>Description</b>
$\rho$	Density
$\mathbf{u}$	Velocity vector
$p$	Pressure
$\mu$	Viscosity
$\mu_T$	Turbulent eddy viscosity
$k$	Turbulent kinetic energy
$\varepsilon$	Turbulent dissipation rate
$P_k$	Production term
$\nu_T (= \frac{\mu_T}{\rho})$	Turbulent (kinetic) eddy viscosity
$l_{mix}$	Mixing length
$\overline{u_i u_j}$	Reynolds' stress tensor
$S_{ij}$	Strain-stress tensor
$\delta_{ij}$	Kronecker delta
$k_0$	Initial turbulent kinetic energy
$\varepsilon_0$	Initial turbulent dissipation rate
$\mathbf{U}$	Initial inlet velocity
$\sigma$	Viscous stress tensor
$\kappa_v$	Von Karman constant
$H$	Step height
$r$	Radius of the obstacle

## List of Tables

**Table 2.1:** Constants used in the model

**Table 3.1:** Grid sensitivity test.

## List of Figures

**Figure 1.1:** Laminar flow through a pipe.

**Figure 1.2:** Turbulent flow through a pipe.

**Figure 1.3:** Smokes rising from a cigarette

**Figure 1.4:** Flight of a cricket ball.

**Figure 1.5:** Air circulation in atmosphere.

**Figure 1.6:** Distribution of  $\bar{u}$  and  $u'$  in turbulent flow.

**Figure 1.7:** A backward facing step.

**Figure 2.1:** Geometry of the flow.

**Figure 2.2:** The computational domain starts at a distance  $\delta_w$  from the wall.

**Figure 3.1:** Magnified view of the mesh elements

**Figure 3.2:** Average velocity versus the number of mesh elements.

**Figure 4.1:** Turbulent dynamic viscosity versus arc length taken along the centerline.

**Figure 4.2:** Stream lines for the different sizes of the circular obstacle: (a) obstacle with radius  $r = H/4$ , (b) obstacle with radius  $r = H/2$  and (c) obstacle with radius  $r = H$ .

**Figure 4.3:** Velocity magnitude for obstacle size with radius  $r = H/4, H/2, H$ .

**Figure 4.4:** Pressure distribution for obstacle size with radius  $r = H/4, H/2, H$ .

**Figure 4.5:** Velocity profiles for three obstacle sizes at the center of the obstacle: (a) obstacle with radius  $r = H/4$ , (b) obstacle with radius  $r = H/2$  and (c) obstacle with radius  $r = H$ .

**Figure 4.6:** Velocity profiles for three obstacle sizes at the downstream ( $x/H = 8$ ): (a) obstacle with radius  $r = H/4$ , (b) obstacle with radius  $r = H/2$  and (c) obstacle with radius  $r = H$ .

**Figure 4.7:** Turbulent kinetic energy for three obstacle sizes at the center of the obstacle: (a) obstacle with radius  $r = H/4$ , (b) obstacle with radius  $r = H/2$  and (c) obstacle with radius  $r = H$ .

**Figure 4.8:** Turbulent kinetic energy for three obstacle sizes at the downstream ( $x/H = 8$ ): (a) obstacle with radius  $r = H/4$ , (b) obstacle with radius  $r = H/2$  and (c) obstacle with radius  $r = H$ .

**Figure 4.9:** Turbulent dissipation rate for three obstacle sizes at the center of the obstacle: (a) obstacle with radius  $r = H/4$ , (b) obstacle with radius  $r = H/2$  and (c) obstacle with radius  $r = H$ .

**Figure 4.10:** Turbulent dissipation rate for three obstacle sizes at the downstream ( $x/H = 8$ ): (a) obstacle with radius  $r = H/4$ , (b) obstacle with radius  $r = H/2$  and (c) obstacle with radius  $r = H$ .

**Figure 4.11:** Stream lines for the different positions of the circular obstacle with size  $r = H/2$ : (a) obstacle with center at distance  $H$  from step, (b) obstacle with center at distance  $3H$  from step and (c) obstacle with center at distance  $5H$  from step.

**Figure 4.12:** Velocity magnitude for the different positions of the circular obstacle with size  $r = H/2$ : (a) obstacle with center at distance  $H$  from step, (b) obstacle with center at distance  $3H$  from step and (c) obstacle with center at distance  $5H$  from step.

**Figure 4.13:** Pressure distribution for obstacle positions with radius  $H/2$  at: (a) obstacle with center at distance  $H$  from step, (b) obstacle with center at distance  $3H$  from step and (c) obstacle with center at distance  $5H$  from step.

**Figure 4.14:** Velocity profiles for three obstacle positions at the center of the obstacle: (a) obstacle at position  $x/H = 1$ , (b) obstacle at position  $x/H = 3$  and (c) obstacle at position  $x/H = 5$ .

**Figure 4.15:** Velocity profiles for three obstacle positions at the downstream ( $4H$  from the obstacle): (a) obstacle at position  $x/H = 1$ , (b) obstacle at position  $x/H = 3$  and (c) obstacle at position  $x/H = 5$ .

**Figure 4.16:** Turbulent kinetic energy for three obstacle positions at the center of the obstacle: (a) obstacle at position  $x/H = 1$ , (b) obstacle at position  $x/H = 3$  and (c) obstacle at position  $x/H = 5$ .

**Figure 4.17:** Turbulent kinetic energy for three obstacle positions at the downstream ( $4H$  from the obstacle): (a) obstacle at position  $x/H = 1$ , (b) obstacle at position  $x/H = 3$  and (c) obstacle at position  $x/H = 5$ .

**Figure 4.18:** Turbulent dissipation rate for three obstacle positions at the center of the obstacle: (a) obstacle at position  $x/H = 1$ , (b) obstacle at position  $x/H = 3$  and (c) obstacle at position  $x/H = 5$ .

**Figure 4.19:** Turbulent dissipation rate for three obstacle positions at the downstream ( $4H$  from the obstacle): (a) obstacle at position  $x/H = 1$ , (b) obstacle at position  $x/H = 3$  and (c) obstacle at position  $x/H = 5$ .

# Chapter 1

## Introduction

### ***1.1 Basic Concepts: Laminar and Turbulent Flows***

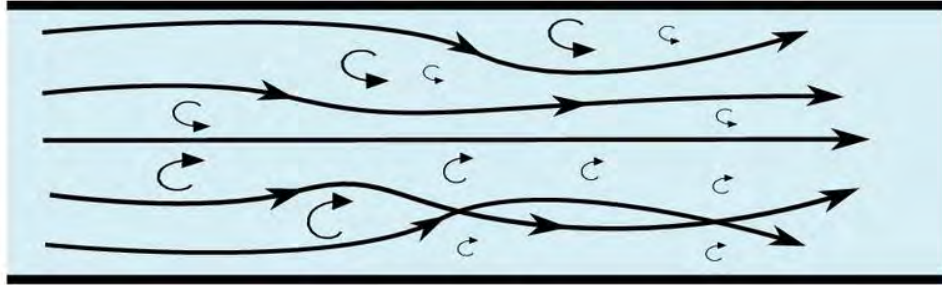
The motion of fluids caused by unbalanced forces or stresses is called the fluid flow. This motion continues as long as the unbalanced forces act on the fluid. Generally two types of flows are there namely the laminar flow and the turbulent flow. The laminar flow occurs when the fluid flows in parallel layers, with no mixing between the layers. In this case the center of the pipe has the fastest flow and at the wall the flow is stalled with no slip condition. The currents do not cross each other and there is no component perpendicular to the direction of the flow. The motion of the fluid particles is very orderly and systematic. High momentum diffusion and low momentum convection characterizes the laminar flow regime.



**Figure 1.1:** Laminar flow through a pipe.

On the other hand, the irregular motion of the fluid is generally known as the turbulence or turbulent flow which occurs in most of the natural or physical phenomena. Although laminar flow is commonly studied by scientists and engineers it is in fact a rare occurrence in the nature. Almost in all of the cases the flow at some stage becomes turbulent. In turbulent flow variables like

velocity, density and pressure etc. are random variables having some mean values. The following section discusses in detail about turbulence.



**Figure 1.2:** Turbulent flow through a pipe.

## ***1.2 General Properties of Turbulence***

### ***The Basic Definition***

In 1937 von Karman defined turbulence in a presentation at the Twenty Fifth Wilbur Wright Memorial Lecture entitled “Turbulence.” He quoted G. I. Taylor as follows (von Karman (1937)):

*“Turbulence is an irregular motion which in general makes its appearance in fluids, gaseous or liquid, when they flow past solid surfaces or even when neighboring streams of the same fluid flow past or over one another.”*

With the progress of the understanding of turbulence, scientists have found the term “*irregular motion*” to be very imprecise. The simple definition says that an irregular motion is one that is typically aperiodic and that cannot be described as a regular function of time and space coordinates. An irregular motion may also depend strongly and sensitively upon the initial conditions. The problem with the Taylor-von Karman definition of turbulence lies in the fact that there are nonturbulent flows that can be described as irregular.

Turbulent motion is indeed irregular in the sense that it can be described by the laws of probability. Although instantaneous properties in a turbulent flow are extremely sensitive to initial conditions, statistical averages of the instantaneous properties are not.

To provide a sharper definition of turbulence, Hinze (1975) offers the following revised definition:

*“Turbulent fluid motion is an irregular condition of flow in which the various quantities show a random variation with time and space coordinates, so that statistically distinct average values can be discerned.”*

To complete the definition of turbulence, Bradshaw [Cebeci and Smith (1974)] adds the statement that *“turbulence has a wide range of scales.”* Time and length scales of turbulence are represented by frequencies and wavelengths that are revealed by a Fourier analysis of a turbulent flow time history.

The irregular nature of turbulence stands in contrast to laminar motion, so called historically because the fluid was imagined to flow in smooth layers. To describe turbulence, many researchers refer to eddying motion, which is a local swirling motion where the vorticity can often be very severe. The eddies appear in a wide range of sizes and give rise to extensive mixing and effective turbulent stresses which is large compared to laminar values.

### ***Instability and Nonlinearity***

Analysis of solutions to the Navier-Stokes equation, or more typically to its boundary layer form, shows that turbulence develops as an instability of laminar flow. To analyze the stability of laminar flows, classical methods begin by linearizing the equations of motion. Although linear theories achieve some degree of success in predicting the onset of instabilities that ultimately lead to turbulence, the inherent nonlinearity of the Navier-Stokes equations precludes a

complete analytical description of the actual transition process, let alone the fully turbulent state. For a real fluid, mathematically speaking, the instabilities result mainly from interaction between the Navier-Stokes equations' nonlinear inertial terms and viscous terms. The interaction is very complex in nature.

As an overview, the nonlinearity of the Navier-Stokes equations lead to interactions between fluctuations of differing wavelengths and directions. The wavelengths of the motion usually extend all the way from a maximum comparable to the width of the flow to a minimum fixed by viscous dissipation of energy. The main physical process that spreads the motion over a wide range of wavelengths is vortex stretching. The turbulence gains energy if the vortex elements are primarily oriented in a direction in which the mean velocity gradients can stretch them. Most importantly, wavelengths that are not too small compared to the mean flow width interact most strongly with the mean flow. Consequently, the larger scale turbulent motion carries most of the energy and is mainly responsible for the enhanced diffusivity and attending stresses. In turn the larger eddies randomly stretch the vortex elements that comprise the smaller eddies, cascading energy to them. Energy is dissipated by viscosity in the shortest wavelengths, although the rate of dissipation of energy is set by long wavelengths motion at the start of the cascade. The shortest wavelengths simply adjust accordingly.

### ***Turbulence is a Continuum Phenomenon***

In principle the time dependent, three dimensional continuity and Navier-Stokes equations contain all the physics of a given turbulent flow. It is true from the fact that turbulence is a continuum phenomenon. As noted by Tennekes and Lumely (1983),

*“Even the smallest scales occurring in a turbulent flow are ordinarily far larger than any molecular length scale.”*



However, the smallest scales of turbulence are still extremely small. They are generally many orders of magnitude smaller than the largest scale of turbulence, the latter often being of the same order of magnitude as the dimension of the object about which the fluid is flowing. Furthermore, the ratio of smallest to largest scales decreases rapidly as the Reynolds number increases. To make an accurate numerical simulation of a turbulent flow, all physically relevant scales must be resolved.

### ***Turbulence scales and the cascade***

Turbulence consists of a continuous spectrum of scales ranging from largest to smallest, as opposed to a discrete set of scales. In order to visualize a turbulent flow with a spectrum of scales we often cast the discussion in terms of eddies. A turbulent eddy can be thought of as a local swirling motion whose characteristic dimension is the local turbulence scale. It is observed that eddies overlap in space, large ones carrying smaller ones. Turbulence features a cascade process whereby, as the turbulence decays, its kinetic energy transfers from larger eddies to smaller eddies. Ultimately, the smallest eddies dissipate into heat through the action of molecular viscosity. Thus, like any viscous flow, turbulent flows are always dissipative.

### ***Large eddies and turbulent mixing***

An especially striking feature of a turbulent flow is the way large eddies migrate across the flow, carrying smaller scale disturbances with them. The arrival of these large eddies near the interface between the turbulent region and nonturbulent fluid distorts the interface into a highly convoluted shape. In addition to, migrating across the flow, they have a lifetime so long that they persist for distances as much as 30 times the width of the flow (Bradshaw, 1972). Hence the state of a turbulent flow at a given position depends upon

upstream history and cannot be uniquely specified in terms of the local strain rate tensor as in laminar flow.

Enhanced diffusivity is another important feature of turbulence. Turbulent diffusion greatly enhances the transfer of mass, momentum and energy. Apparent stresses in turbulent flows are often several orders of magnitude larger than laminar flows.

The Reynolds number is a non-dimensional quantity which measures the trend of a laminar flow to develop into turbulent flow. The Reynolds number is defined as:

$$\text{Re} = \frac{\rho UL}{\mu}$$

Here  $\rho$  is the density,  $U$  is the velocity of the fluid,  $L$  is the characteristic length and  $\mu$  is the viscosity. If the value of Re is less than 2300 the flow remains laminar and when it gets larger than 4000 the flow becomes turbulent [Holman, 2002]. If the value of Re is between 2300 and 4000 the flow is in a transitional stage where it starts to convert from laminar into turbulent nature depending on the geometry. If the viscosity of the fluid in the pipe or channel is small then the irregular motion develops quicker than when the viscosity is high.

### ***1.3 Examples of Turbulence***

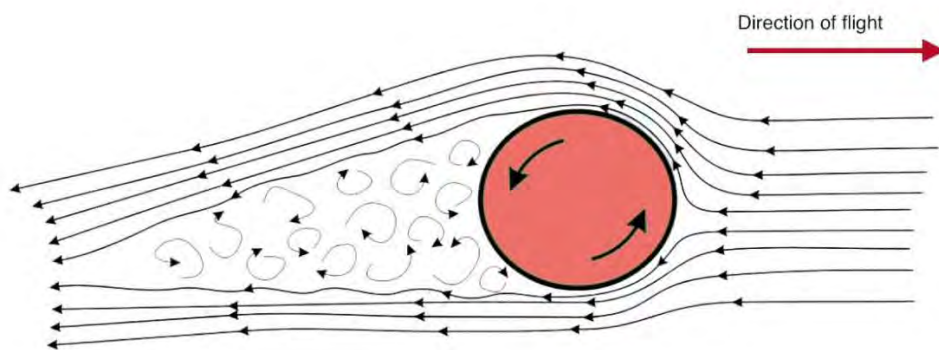
A lot of flows occurring naturally or other ways are turbulent. The flows we observe in our surroundings are mostly turbulent. Following are a few examples of turbulent flow:

Smoke rising from a cigarette is mostly turbulent. However, for the few centimeters the flow is laminar. The plume becomes turbulent as the Reynolds number increases due to its velocity and characteristic length.



**Figure 1.3:** Smokes rising from a cigarette

The flow over a cricket ball is turbulent. This can be best understood if the ball is considered stationary and the air is flowing over it. If the cricket ball is considered smooth, the boundary layer flow over the front of the sphere would be laminar at typical conditions. But the boundary layer would separate early, as the pressure gradient switched from favorable to unfavorable, creating a large region of low pressure behind the ball that creates high form drag. To prevent this from happening the surface is covered by seam to perturb the boundary layer and promote transition to turbulence. This results in higher skin friction, but moves the point of boundary layer separation further along, resulting in lower form drag and lower overall drag.



**Figure 1.4:** Flight of a cricket ball.

During an airplane flight and in poor astronomical seeing, clear air turbulence is observed. Most of the terrestrial atmospheric circulation is turbulent. The oceanic and atmospheric intensive mixed layers are turbulent.

Other examples of turbulence are:

The flow conditions in many industrial equipment (such as pipes, ducts, precipitators, gas scrubbers, dynamic scraped surface heat exchangers, etc.) and machines (for instance, internal combustion engines and gas turbines).

The external flow over all kind of vehicles such as cars, airplanes, ships and submarines.

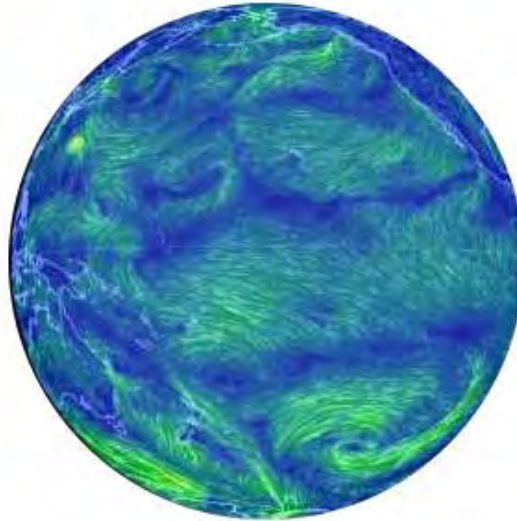
The motions of matter in stellar atmospheres.

A jet exhausting from a nozzle into a quiescent fluid. As the flow emerges into this external fluid, shear layers originating at the lips of the nozzle are created. These layers separate the fast moving jet from the external fluid, and at a certain critical Reynolds number they become unstable and break down to turbulence.

Biologically generated turbulence resulting from swimming animals affects ocean mixing.

The motion of clouds in the upper atmosphere.

The motion of water in the water falls, dam or rivers.



**Figure 1.5:** Air circulation in atmosphere.

### ***1.4 Describing the Turbulent Flow***

The Navier-Stokes equations which describe all the flow of fluids can also be used to depict the turbulent flow. But this will require a huge computational cost and time. Because all the scales from the largest to the smallest will have to be resolved which do not facilitate economy at all. A good alternative is to separate the larger and smaller scales where the larger scales are resolved and the smaller scales are modeled. The target of this turbulence model is to be much less expensive than the fully resolved flows. There are several types of turbulent models based on the modification on the Navier-Stokes equations. The modification is called the Reynolds averaging procedure and the resulting equations are called the Reynolds-Averaged Navier-Stokes (RANS) equations. The models based on this averaging are classified as the zero equation model, one equation model and two equations model. The model in which two additional equations are supplemented with the RANS equations is called a two equation model. If one additional equation is used then it is called one equation model and no additional equation gives the zero equation model. The Reynolds-averaging procedure is briefly discussed below.

In this process a quantity is resolved into two parts: the time-averaged part and the fluctuating part. For example if  $u$  is the velocity component of the fluid then it is written as:

$$u = \bar{u} + u'$$

where  $\bar{u}$  is the averaged part and  $u'$  is the fluctuating part. The average of the fluctuating part is assumed to be zero, i. e.,  $\overline{u'} = 0$

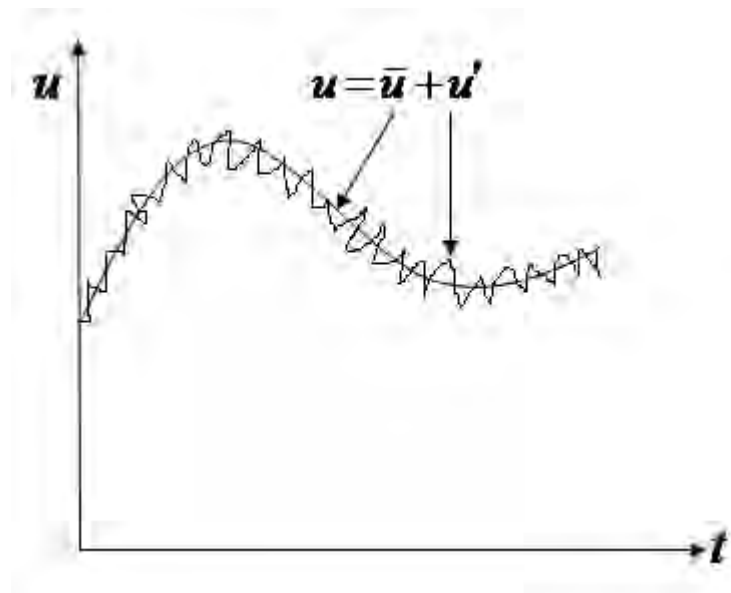
so that

$$\overline{u} = \overline{\bar{u} + u'} = \overline{\bar{u}} + \overline{u'} = \bar{u} + 0 = \bar{u}$$

Some other basic properties of the averaging procedure are:

$$\overline{u + v} = \bar{u} + \bar{v}, \quad \overline{\bar{u}} = \bar{u}, \quad \overline{\bar{u} v} = \bar{u} \bar{v},$$

$$\overline{\bar{u} v} = \bar{u} \bar{v}, \quad \overline{\bar{u} v'} = 0, \quad \frac{\partial \bar{u}}{\partial x} = \frac{\partial \bar{u}}{\partial x}.$$



**Figure 1.6:** Distribution of  $\bar{u}$  and  $u'$  in turbulent flow.

To describe turbulent flow two types of averages are considered:

- i) Average with respect to time
- ii) Average with respect to space

Time average of velocity (mean velocity at time  $t$ ) can be calculated as:

$$\bar{u} = \frac{1}{T} \int_{t-\frac{T}{2}}^{t+\frac{T}{2}} u dt$$

where  $T$  is the time scale of average.

The incompressible Navier-Stokes equations for a Newtonian fluid are (in vector form):

$$\nabla \cdot \mathbf{u} = 0$$

$$\mathbf{u}_t + \mathbf{u} \cdot \nabla \mathbf{u} = -\nabla p + \nu \Delta \mathbf{u}$$

The equations are written here without the body-force term.

From the continuity equation we get,

$$\nabla \cdot \mathbf{u} = \nabla \cdot (\bar{\mathbf{u}} + \mathbf{u}') = \nabla \cdot \bar{\mathbf{u}} + \nabla \cdot \mathbf{u}' = 0$$

Averaging this equation results in

$$\nabla \cdot \bar{\mathbf{u}} + \nabla \cdot \bar{\mathbf{u}'} = 0$$

which means we have,  $\nabla \cdot \bar{\mathbf{u}} = 0$  or  $\nabla \cdot \mathbf{u} = 0$  (discarding the bar sign).

In a similar manner applying the same decomposition and averaging procedure in the momentum equation we get

$$\frac{\partial \mathbf{u}}{\partial t} + \mathbf{u} \cdot \nabla \mathbf{u} + \nabla (\overline{\mathbf{u}' \otimes \mathbf{u}'}) = -\frac{1}{\rho} \nabla p + \nabla \cdot \nu (\nabla \mathbf{u} + (\nabla \mathbf{u})^T)$$

Here  $\otimes$  represents the outer vector product. The last term on the left hand side is a new term comparing to the original Navier-Stokes equations. The term is called the Reynolds stress tensor which represents the relations between the fluctuating velocities. To model the flow this term is needed to deal with.

Treating the turbulent flow in absolutely diffusive mode is one of best way to good modeling.

Joseph Valentin Boussinesq was the first to attack the closure problem, by introducing the concept of eddy viscosity. In 1877 Boussinesq proposed that the Reynolds stresses could be linked to the mean rate of deformation. The Boussinesq hypothesis is applied to model the Reynolds stress term.

The Reynolds stress tensor is thus denoted by

$$\nabla (\overline{\mathbf{u}' \otimes \mathbf{u}'}) - \frac{\rho}{3} \text{trace} (\overline{\mathbf{u}' \otimes \mathbf{u}'}) = -\mu_T (\nabla \mathbf{u} + (\nabla \mathbf{u})^T)$$

where  $\mu_T$  is the turbulent viscosity or the eddy viscosity.

The turbulent viscosity depends on the flow, i.e. the state of turbulence. The turbulent viscosity is not homogeneous, i.e. it varies in space.

Due to this term sometimes the models using this term are called the “eddy viscosity models”.



The second term on the left side of the above equation is added to make it applicable to normal turbulent stress and can be written in the form

$$\frac{\rho}{3} \text{trace}(\overline{\mathbf{u}' \otimes \mathbf{u}'}) = \frac{2}{3} \rho k$$

Here  $k$  is the turbulent kinetic energy.

The two equation models are most popular to describe the turbulent flow. Of them the  $k-\varepsilon$  model and the  $k-\omega$  model are prominent. There are several other two equations models also.

## ***1.5 $k - \varepsilon$ Turbulence Model***

The  $k-\varepsilon$  turbulence model is the most common model to describe the turbulent flow. It can simulate the mean flow characteristics very well for turbulent flow conditions. This two equation model gives a general description of turbulence by means of two additional transport equations. Although, the original aim for the  $k-\varepsilon$  model was to improve the mixing length model, as well to find an alternative to algebraically prescribing turbulent length scales in moderate to highly complex flows, it has exceeded its target far better than projected.

Turbulent kinetic energy( $k$ ) is the first transported variable which determines the energy in the turbulence. The second transported variable is the turbulent dissipation rate( $\varepsilon$ ) which determines the rate of dissipation of the turbulent kinetic energy. Unlike earlier turbulence models,  $k-\varepsilon$  model focuses on the mechanisms that affect the turbulent kinetic energy. The underlying assumption of this model is that the turbulent viscosity is isotropic, i. e. the ratio between the Reynolds stress and mean rate of deformations is the same in all directions.

The exact  $k - \varepsilon$  equations contain many unknown and unmeasurable terms. For a much more practical approach, the standard  $k - \varepsilon$  turbulence model is used which is based on the understanding of the relevant processes, thus minimizing unknowns and presenting a set of equations which can be applied to a large number of turbulent applications.

The transport equations are as follows:

$$\rho \frac{\partial k}{\partial t} + \rho \mathbf{u} \cdot \nabla k = \nabla \cdot \left( \left( \mu + \frac{\mu_T}{\sigma_k} \right) \nabla k \right) + P_k - \rho \varepsilon$$

$$\rho \frac{\partial \varepsilon}{\partial t} + \rho \mathbf{u} \cdot \nabla \varepsilon = \nabla \cdot \left( \left( \mu + \frac{\mu_T}{\sigma_\varepsilon} \right) \nabla \varepsilon \right) + \frac{\varepsilon}{k} (C_1 P_k - C_2 \varepsilon)$$

In the above two equations the format is as follows:

*Rate of change of  $k$  or  $\varepsilon$  + Transport of  $k$  or  $\varepsilon$  by convection  
= Transport of  $k$  or  $\varepsilon$  by diffusion + Rate of production – Rate of destruction*

Here the production term  $P_k$  is given by

$$P_k = \frac{\mu_T}{2\rho} (\nabla \mathbf{u} + \nabla \mathbf{u}^T)^2$$

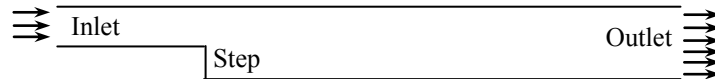
In the standard  $k - \varepsilon$  model, the turbulent eddy viscosity  $\nu_T (= \frac{\mu_T}{\rho})$  is defined by

$$\mu_T = \rho C_\mu \frac{k^2}{\varepsilon} \quad \text{or} \quad \nu_T = C_\mu \frac{k^2}{\varepsilon}$$

## **1.6 Backward Facing Step**

In a backward facing step the inlet channel is narrower than the outlet channel and there is a sudden step in the flow field. The flow separates at the step and reattaches again down the stream. If the flow velocity is sufficiently high then

the Reynolds number also becomes high and the flow becomes turbulent after separation. A lot of turbulent models and conditions are tested on the backward facing step. This is a benchmark geometry to study various fluid flow models and conditions.



**Figure 1.7:** A backward facing step

## ***1.7 Historical Background and Literature Review***

Primarily this work is based upon the Reynolds-Averaged Navier-Stokes equations. The origin of this approach dates back to the end of the nineteenth century when Reynolds (1895) published results of his research on turbulence. His pioneering work proved to have such profound importance for all future developments that we refer to the standard time-averaging process as one type of Reynolds averaging.

The earliest attempts at developing a mathematical description of turbulent stresses sought to mimic the molecular gradient-diffusion process. In this essence, Boussinesq (1877) introduced the concept of a so-called eddy viscosity. As with Reynolds, Boussinesq has been immortalized in turbulence literature. The Boussinesq eddy viscosity approximation is so widely known that few authors find a need to reference his original paper.

Neither Reynolds nor Boussinesq attempted a solution of the Reynolds-averaged Navier-Stokes equation in any orderly manner. Much of the physics of

viscous flows was a mystery in the nineteenth century, and additional progress waited for the discovery of boundary layer by Prandtl in 1904. Keeping a focus upon the turbulent flows, Prandtl (1925) introduced the mixing-length (an analog of the mean free path of a gas) and a straightforward prescription for computing the eddy viscosity in terms of the mixing length. The mixing length hypothesis, very close to the eddy viscosity concept, formed the basis of virtually all turbulence modeling research for the next twenty years. Several researchers made some important early contributions, most notable of them is von Karman (1930). In present days the model based on the mixing length theory is referred as an algebraic model or a zero equation model. As stated above, an  $n$ -equation model signifies a model that requires solution of  $n$  additional differential transport equations in addition to those expressing conservation of mass, momentum and energy for the mean flow.

To improve the ability to predict properties of turbulent flows and to develop a more realistic mathematical description of the turbulent stresses, Prandtl (1945) postulated a model in which the eddy viscosity depends upon the kinetic energy of the turbulent fluctuations,  $k$ . He proposed a modeled partial differential equation approximating the exact equation for  $k$ . This improvement, on a conceptual level, takes account of the fact that the turbulent stresses and thus the eddy viscosity, are affected by where the flow has been, i. e. upon flow history. Thus the one equation model of turbulence was born.

While having an eddy viscosity that depends upon flow history provides a more physically realistic model, the need to specify a turbulence length scale remains. That is, on dimensional grounds, viscosity has dimensions of velocity multiplied by length. Since the length scale can be thought of as a characteristic eddy size and since such scales are different for each flow, turbulence models that do not provide a length scale are incomplete. That is, we must know something about

the flow, other than initial and boundary conditions, in advance in order to obtain a solution. Incomplete models are not without merit and, in fact, have proven to be of great value in many engineering applications. To elaborate a bit further, an incomplete model generally defines a turbulence length scale in a prescribed manner from the mean flow for an attached boundary layer. However, a different length scale would be needed when the boundary layer separates. Yet another length might be needed for the free shear flows. In essence, incomplete models usually define quantities that may vary more simply or more slowly than the Reynolds stresses (i. e. eddy viscosity and mixing length). Presumably such quantities would prove to be much easier to correlate than the actual stresses.

A particularly desirable type of turbulence model would be one that can be applied to a given turbulent flow by prescribing at most the appropriate boundary and/ or initial conditions. Ideally no advance knowledge of any property of the turbulence should be required to obtain a solution. Such type of model is defined as complete. It is to be noted that this definition implies nothing regarding the accuracy or universality of the model, only that it can be used to determine a flow with no prior knowledge of any flow details.

Kolmogorov (1942) introduced the first complete model of turbulence. In addition to having a modeled equation for  $k$ , he introduced a second parameter  $\omega$  that he referred to as “the rate of dissipation of energy in unit volume and time.” The reciprocal of  $\omega$  serves as turbulence time scale, while  $\frac{k^{1/2}}{\omega}$  serves as the analog of the mixing length and  $k\omega$  is the analog of the dissipation rate  $\varepsilon$ . In this model known as  $k-\omega$  model,  $\omega$  satisfies a differential equation somewhat similar to the equation for  $k$ . The model is thus termed a two equation model of turbulence. While this model offered great promise, it went

with virtually no applications for the next quarter century. Chou (1945) and Rotta (1951) laid the foundation for turbulence models that obviate use of the Boussinesq approximation. Rotta devised a plausible model for the differential equation governing evolution of tensor that represents the turbulent stresses, i. e., the Reynolds stress tensor. Such models are most appropriately described as stress-transport models. Many authors refer to this approach as second order closure. The primary conceptual advantages of stress transport model is the natural manner in which non local and history effects are incorporated.

Although quantitative accuracy often remains difficult to achieve, such models automatically accommodate complicating effects such as sudden changes in strain rate, streamline curvature, rigid body rotation, and body forces. This stands in distinct contrast to eddy viscosity models that account of these effects only if empirical terms are added.

Some surveying has been done and it is found in the literature that some important and very crucial investigations are done regarding the  $k-\varepsilon$  turbulence model and backward facing step. Kuzmin et al. (2007) studied the standard  $k-\varepsilon$  turbulence model on the backward facing step with various boundary conditions. They used a positivity constraint to get convergent solutions. Wilcox (2006) in his renowned book "Turbulence Modeling for CFD" discussed in detail about the development and description of the turbulence models and their various aspects and the technique to solve these models numerically using computer programs.

While Kolmogorov's  $k-\omega$  model was the first of this kind, it remained in obscurity until the computers became available. By far the most extensive work on two equation models has been done by Launder and Spalding (1974) who

devised a  $k-\varepsilon$  turbulence model which is recognized as the standard  $k-\varepsilon$  turbulence model. Abe et al. (1994) formulated a low Reynolds number  $k-\varepsilon$  turbulence model to calculate separating and re-attaching flows. Lasher and Taulbee (1992) applied Reynolds stress model to study the turbulent back-step flow. Driver and Seegmiller (1985) experimentally studied a rear-ward facing divergent channel flow. Kim (1978) investigated the separation and reattaching of the turbulent shear layer flow over a backward facing step. Very recently Jehad et al. (2015) studied different turbulence models numerically over a backward facing step and Ratha et al. (2015) studied turbulent flow over a modified backward facing step with transition.

Lew et al. (2001) used a decoupling technique in the transport equations of the  $k-\varepsilon$  model to simplify them further. Utnes et al. (1988) studied the two equation turbulence model using a finite element outline. Ilinca et al. (1997A) studied how to preserve positivity and adapt the solution of a  $k-\varepsilon$  turbulence model. Ilinca et al. (1997B) studied a finite element scheme for the free shear flows in turbulence. Codina and Soto (1999) investigated finite element implementation on the two equation and algebraic stress models for turbulent flow.

## ***1.8 Motivation***

From the above section it is observed that a lot of research and studies were done on the backward facing step flow using turbulence models. Different models with various boundary conditions and numerical techniques were used to study the flow in the geometry shown in Figure 1.7. In those studies nobody considered any obstacle inside the backward facing step, but in the present study a circular shaped obstacle is considered at the downstream of the step.

## ***1.9 Objectives***

The objectives of the present study is as follows:

- To study the standard  $k-\varepsilon$  turbulence model on backward facing step with an obstacle.
- To investigate the effect of the size and position of the obstacle on the flow pattern inside the geometry.
- To visualize the stream lines, velocity magnitudes, pressure distribution, velocity profiles, turbulent kinetic energy and turbulent dissipation rate etc. on the flow field.



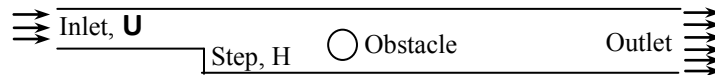
## Chapter 2

### Formulation

#### 2.1 Problem Formulation

The intention is to study the turbulent flow over a backward facing step by modifying the geometry. To study the turbulent flow the standard  $k-\varepsilon$  model has been chosen. The modification in the geometry is that a circular solid obstacle has been placed at the downstream of the backward step. The step height  $H$  is taken as the half of the inlet channel height.

The figure of the geometry is given below:



**Figure 2.1:** Geometry of the flow.

The flow will enter from the left at the inlet with velocity  $\mathbf{U}$ . Then it will go past the step and the obstacle. Finally the flow will go out through the outlet. In the geometry a circular obstacle is placed which is centered at a distance  $5H$  ( $H$  is the step height) from the step and has a radius  $H/2$ . The vertical coordinate of the center of the circle has been taken in the middle of the channel. In Sections 4.1 and 4.2 the flow field using variations in the distance and size of the obstacle will be studied.

## 2.2 Mathematical Model

The hydrodynamic/ hydrokinetic behavior of a turbulent flow can be portrayed by the eddy viscosity models using the RANS equations for the velocity and pressure denoted by  $\mathbf{u}$  and  $p$  respectively as follows:

$$\rho \nabla \cdot \mathbf{u} = 0 \quad (1)$$

$$\rho \frac{\partial \mathbf{u}}{\partial t} + \rho \mathbf{u} \cdot \nabla \mathbf{u} = -\rho \nabla p + \nabla \cdot [(\mu + \mu_T)(\nabla \mathbf{u} + \nabla \mathbf{u}^T)] \quad (2)$$

The equation (1) is the continuity equation and the equation (2) is the momentum equation.

In the  $k-\varepsilon$  model two additional transport equations for turbulent kinetic energy  $k$  and turbulent dissipation rate  $\varepsilon$  are introduced to complement the above equations. These are:

$$\rho \frac{\partial k}{\partial t} + \rho \mathbf{u} \cdot \nabla k = \nabla \cdot \left( \left( \mu + \frac{\mu_T}{\sigma_k} \right) \nabla k \right) + P_k - \rho \varepsilon \quad (3)$$

$$\rho \frac{\partial \varepsilon}{\partial t} + \rho \mathbf{u} \cdot \nabla \varepsilon = \nabla \cdot \left( \left( \mu + \frac{\mu_T}{\sigma_\varepsilon} \right) \nabla \varepsilon \right) + \frac{\varepsilon}{k} (C_1 P_k - C_2 \varepsilon) \quad (4)$$

Here the production term  $P_k$  is given by

$$P_k = \frac{\mu_T}{2\rho} (\nabla \mathbf{u} + \nabla \mathbf{u}^T)^2 \quad (5)$$

In the standard  $k-\varepsilon$  model, the turbulent eddy viscosity  $\nu_T (= \frac{\mu_T}{\rho})$  is defined by

$$\mu_T = \rho C_\mu \frac{k^2}{\varepsilon} \quad \text{or} \quad \nu_T = C_\mu \frac{k^2}{\varepsilon} \quad (6)$$

The values for the empirical constants [Kuzmin, 2007] are:

**Table 2.1:** Constants used in the model

Constants	$C_\mu$	$C_1$	$C_2$	$\sigma_k$	$\sigma_\varepsilon$
Values	0.09	1.44	1.92	1.0	1.3

It is difficult to solve the equations (3)-(5) directly. Preventing the division by zero during the solution process is almost impossible. An upper limit  $l_{mix}^{lim}$  in the mixing length is introduced [Kuzmin, 2007].

$$l_{mix} = \max\left(C_\mu \frac{k^2}{\varepsilon}, l_{mix}^{lim}\right) \quad (7)$$

Turbulent viscosity is calculated using this mixing length. A converged solution does not use this upper limit but it is simply used to obtain convergence.

The Reynolds stress tensor for the eddy viscosity model is written as:

$$\overline{\rho u_i u_j} = -2\mu_T S_{ij} + \frac{2}{3}\rho k \delta_{ij} \quad (8)$$

where  $\delta_{ij}$  is the Kronecker delta and  $S_{ij}$  is the strain-stress tensor. The calculation of  $\mu_T$  from equation (6) does not guarantee the non-negativity of the diagonal elements of the Reynolds stress tensor which is essential. To make sure that

$$\overline{\rho u_i u_i} > 0$$

a realizability constraint is imposed on the turbulent viscosity. For two dimensional axisymmetry the constraint is:

$$\mu_T \leq \frac{\rho k \sqrt{2}}{3 \sqrt{S_{ij} S_{ij}}} \quad (9)$$

From equations (6), (7), and the definition of the mixing length we obtain the limit of the mixing length as:

$$l_{mix} \leq \sqrt{\frac{2}{3}} \frac{\sqrt{k}}{\sqrt{S_{ij} S_{ij}}} \quad (10)$$

This gives two limitations to the mixing length: limit in (7) and the realizability constraint in (10). Unnecessary turbulence production can be noticed if the realizability constraint is not applied. That is why this constraint is always applied in the RANS models.

### **2.3 Boundary Conditions**

At the initial level it is not so easy to make an appropriate initial guess for the simulations of a turbulent flow. If we take the initial velocity to be zero, then a wastefully large amount of time will be required for the flow to become fully turbulent. That is why the turbulent model comes into action after a while from the startup. The initial values for the  $k$  and  $\varepsilon$  for the turbulent flow are taken as:

$$k_0 = \left( \frac{v_0}{l_0} \right)^2, \quad \varepsilon_0 = C_\mu \frac{k_0^{3/2}}{l_0} \quad ; \text{ at the time before the turbulence}$$

starts.

At the inlet boundary the velocity components and  $k$  and  $\varepsilon$  have the following values:

$$\mathbf{u} = \mathbf{U}, \quad k = c |\mathbf{u}|^2 \quad \text{and} \quad \varepsilon = C_\mu \frac{k_0^{3/2}}{l_0}$$

Here  $c \in (0.003, 0.01)$  is an empirical constant and  $|\mathbf{u}|$  represents the Euclidean norm of the velocity. At the outlet boundary a Neumann condition is imposed which implies that the normal gradients of the variables will vanish:

$$\mathbf{n} \cdot [\nabla \mathbf{u} + \nabla \mathbf{u}^T] = 0, \quad \mathbf{n} \cdot \nabla k = 0 \quad \text{and} \quad \mathbf{n} \cdot \nabla \varepsilon = 0.$$

At an impermeable solid wall the normal component of the velocity is put identical to nil.

$$\mathbf{n} \cdot \mathbf{u} = 0$$

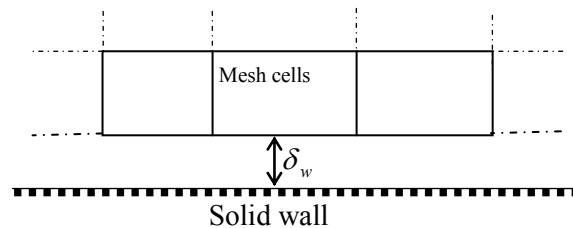
Here the tangential slip is allowed in the simulations of the turbulent flow. In the subsequent step the velocity is projected onto the tangential vector and in the process restrict the defect vector to be zero

$$\mathbf{u} = \mathbf{u}^* - (\mathbf{n} \cdot \mathbf{u}^*) \mathbf{n}$$

After this manipulation the corrected values of  $\mathbf{u}$  act as a Dirichlet boundary condition for the solution at the end of the correction step.

## 2.4 Wall Functions

Very near to the solid walls the turbulent flow is different from that of the free stream flow. Therefore, in the vicinity of the walls the assumptions made for the  $k - \varepsilon$  turbulence model are not applicable all the time. Since it is not very cost-effective to modify the model to describe the flow field near the wall domain, close to the walls some analytical expressions called the wall functions are used as an alternate.



**Figure 2.2:** The computational domain starts at a distance  $\delta_w$  from the wall.

The distance  $\delta_w$  is automatically updated with the formula:

$$\delta_w^+ = \frac{\rho u_T \delta_w}{\mu}$$

where  $u_T = C_\mu^{1/4} \sqrt{k}$  is the friction velocity. The value becomes 11.06 which correspond to the distance from the wall where the logarithmic layer meets the viscous sublayer.  $\delta_w$  is limited from below so that it never becomes smaller than half of the height of the boundary mesh cell.

The constraints for the velocity and shear stress at the boundary are:

$$\mathbf{n} \cdot \mathbf{u} = 0 \text{ and}$$

$$\mathbf{n} \cdot \boldsymbol{\sigma} - (\mathbf{n} \cdot \boldsymbol{\sigma} \cdot \mathbf{n}) \mathbf{n} = -\rho u_\tau \frac{\mathbf{u}}{|\mathbf{u}|} \max(C_\mu^{1/4} \sqrt{k}, u_\tau)$$

where  $\boldsymbol{\sigma} = \mu[\nabla \mathbf{u} + \nabla \mathbf{u}^T]$  is the viscous stress tensor and  $u_\tau = \frac{|\mathbf{u}|}{\frac{1}{\kappa_v \ln \delta_w + B}}$

where in turn  $\kappa_v = 0.41$  is the von Karman constant and  $B$  is another constant having a value of 5.2.

The turbulent kinetic energy has a normal component zero, i. e.,  $\mathbf{n} \cdot \nabla k = 0$ , and the dissipation rate is expressed by:

$$\varepsilon = \frac{C_\mu^{3/4} k^{3/2}}{\kappa_v \delta_w}$$

# Chapter 3

## Methodology

### *3.1 Numerical Scheme*

The finite element method is used to solve the mathematical model for the geometry. There are some advantages of this method over the other methods. The prime advantage of this method is that it can handle complicated geometries with ease. This is the center power of the finite element method. Any complex geometrical shape is discretized into small parts called elements and hence the name. This method can handle a large range of engineering and physical problems having complicated mathematical formulations.

To fill the information gap of a system, experimental setups are made and prototypes need to be built. And this requires a lot of time and investment. An advanced computational tool like the finite element method can come to rescue. It can analyze a problem and obtain the results in a detailed form than the experimental setup can do. Also it is much quicker and the cost is a lot lesser. If the discretized mesh is dense enough the results become very close to the accurate ones. This method can construct broad result sets and produce physical response at any location. Also it can find results in detailed form that might be ignored by the analytical approach. This method can also solve some indeterminate forms.

The numerical technique to solve the system of partial differential equations is based on Galerkin weighted residual method of finite element formulation. At first the solution domain is discretized into finite element meshes of non-uniform elements. Two types of elements are taken in building the mesh. At the free stream the elements are triangular in shape, but near the walls it is observed that the quadrilateral elements give a much better result.

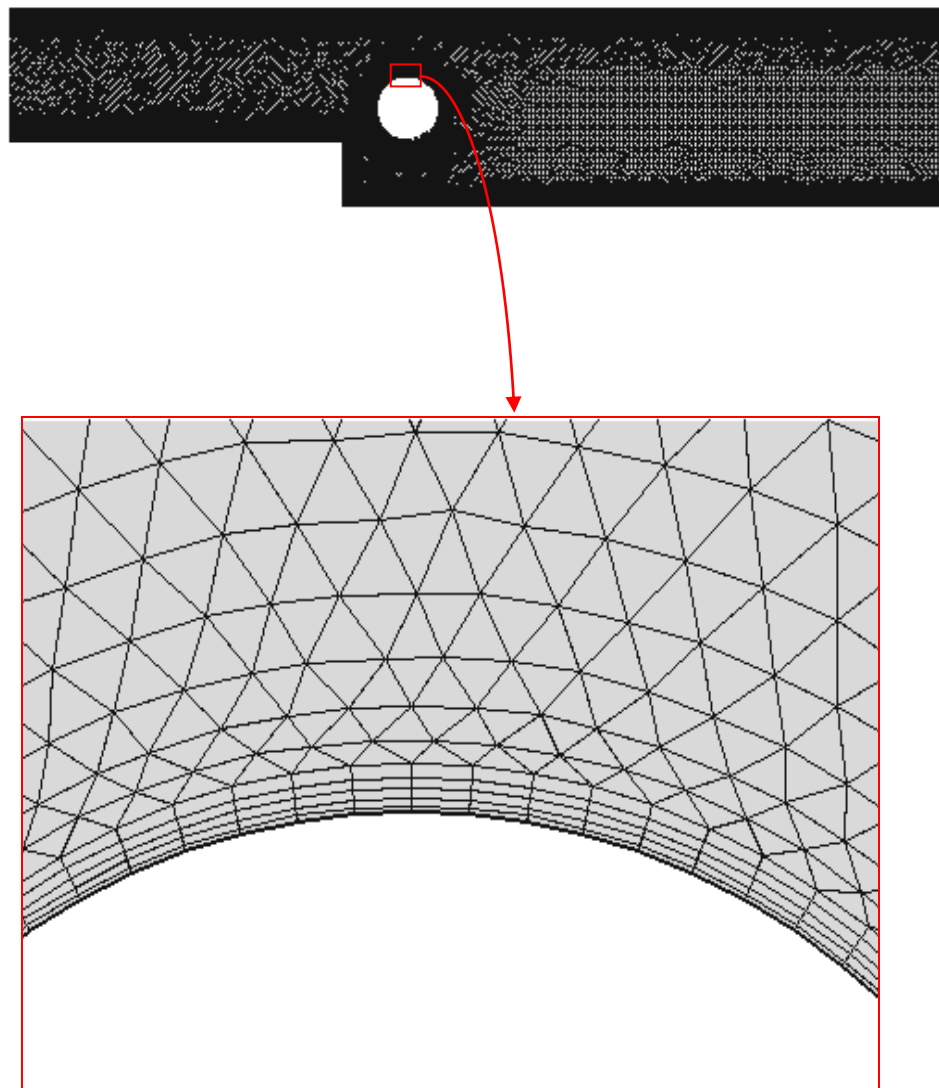
At the next step the nonlinear partial differential equations are transferred into a system of integral equations using weighted Galerkin residual method. Gauss's quadrature technique is used to perform integrations involved in each term. The boundary conditions are imposed to modify the obtained nonlinear algebraic equations. Newton's method is used to convert the system of nonlinear algebraic equations into linear equations. Lastly, this system is solved by triangular factorization method.

The numerical results are presented graphically and / or in tabular form in terms of streamlines, velocity magnitude, pressure, velocity profiles, turbulent kinetic energy profiles and turbulent dissipation rate profiles etc.



### **3.2 Meshes**

The mesh is a small partition of the geometry into small units of a simple form. These units are called the mesh elements. The types of the elements depend on the dimension of the geometry. For example, for a two dimensional geometry the elements can be triangles, quadrilaterals or other two dimensional geometrical shapes. The meshing can be treated as the starting point of the finite element scheme. In the present study the total number of elements is 29665 of which triangular element number is 24086 and rest is other elements.



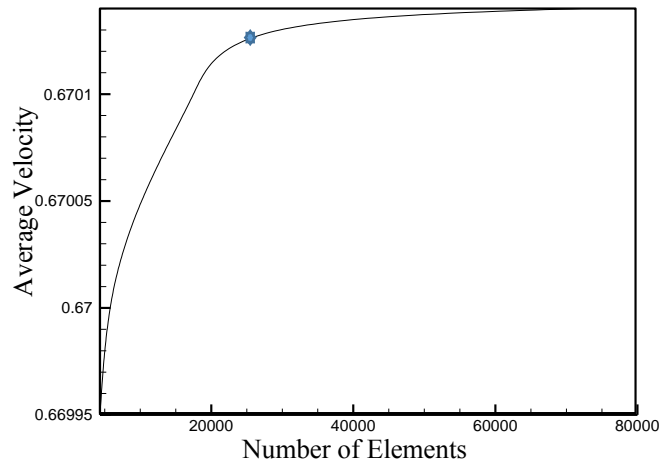
**Figure 3.1:** Magnified view of the mesh elements

### 3.3 Grid Independence Test

To obtain a grid independent solution a grid refinement test was performed. The Table 3.1 and Figure 3.2 describe the result as satisfactory for the grid refinements. In this problem 29665 elements are used for the whole domain. Using more elements are time consuming and do not improve the result significantly.

**Table 3.1:** Grid sensitivity test.

Number of Elements	4330	6326	11520	17483	29665	72108
Time (Sec)	19	31	47	73	137	447
Average Velocity	0.66995	0.67001	0.67006	0.67010	0.67013	0.67015

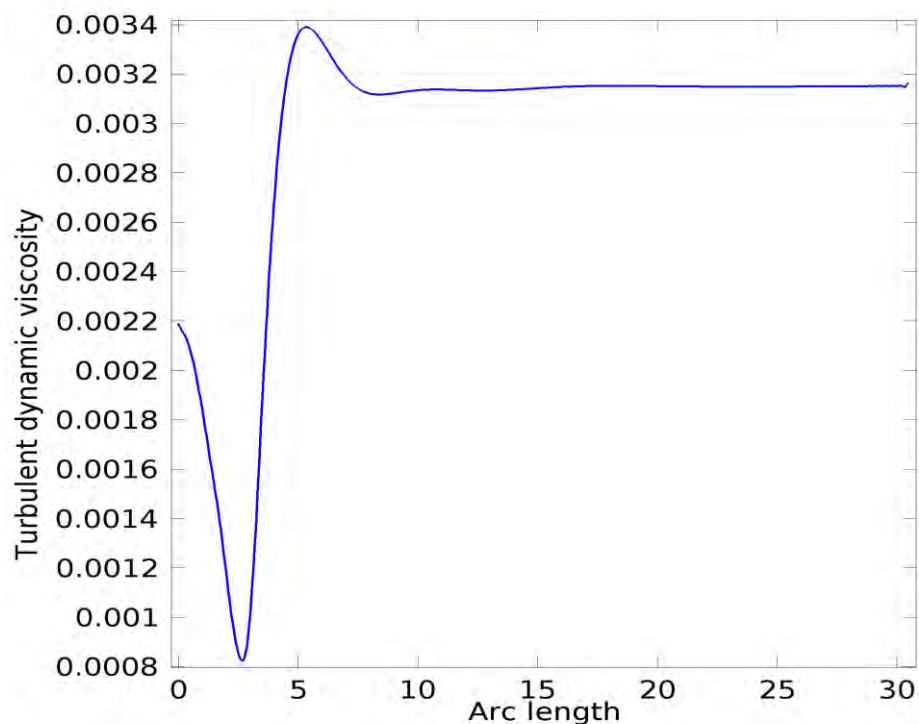


**Figure 3.2:** Average velocity versus the number of mesh elements.

## Chapter 4

### Results and Discussions

To get turbulence in a flow field it is necessary for the flow to be fully developed. In the present work the flow entering the inlet is fully developed and it is clear from the graph in Figure 4.1. This graph shows that the turbulent dynamic viscosity after initially displaying some ups and downs remains constant for rest which is an indication of fully developed flow.



**Figure 4.1:** Turbulent dynamic viscosity versus arc length taken along the centerline.

#### ***4.1 Variation of the Size of the Obstacle***

In this section the effect of some geometrical modifications in the turbulent flow field of the backward facing step are investigated. Effects of obstacle sizes are taken into consideration.

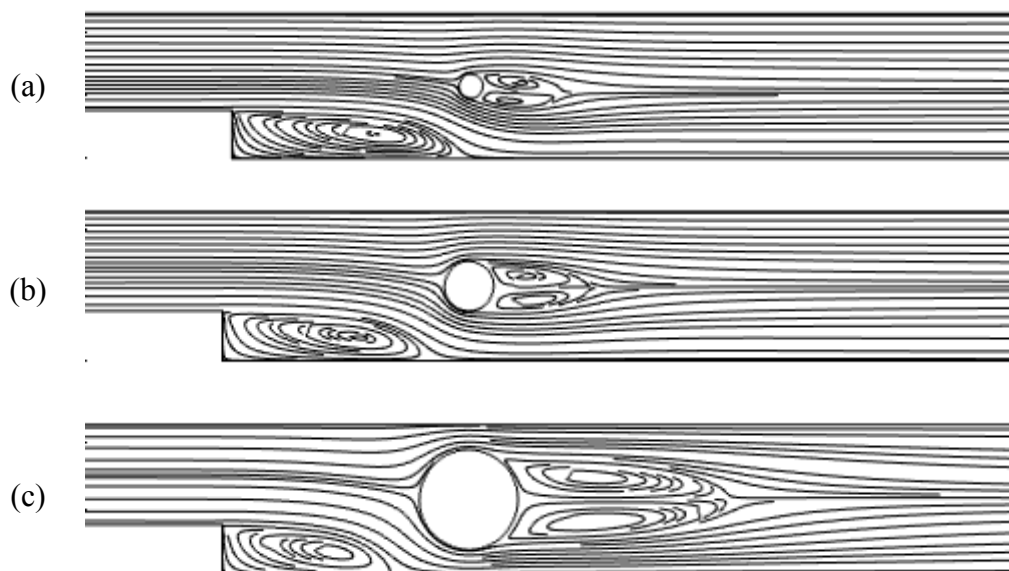
The results are displayed graphically in the form of stream lines, velocity profiles, turbulent kinetic energy profiles, and turbulent dissipation rate profiles for different sizes of the obstacle. The obstacle sizes are chosen as  $r = H/4$ ,  $r = H/2$  and  $r = H$ .

Figure 4.2 represents the stream lines of the flow field for three sizes of the obstacle. For obstacle size  $r = H/4$ , a small vortex forms just after the obstacle which increases in size and length down the stream for larger obstacles. Also it is observed that for the smallest obstacle size only one vortex is produced whereas two vortices are produced for the larger obstacles. In addition, the vortex after the step shows a decreasing trend due to the pressure involved with size of the obstacle. The flow separation that occurs at the step reattaches below the obstacle rapidly when the radius of the circular obstacle is  $H$ . The colored graphs displayed in the Figure 4.3 indicates the velocity magnitude at the various positions of the flow field. The velocity magnitudes at the step and at the wake of the obstacle is much lower as usual. In the Figure 4.4 it is observed that the pressure builds at the lead point of the obstacle as it lowers the passage of the fluid past it in the geometry and obtains the highest value for the largest one.

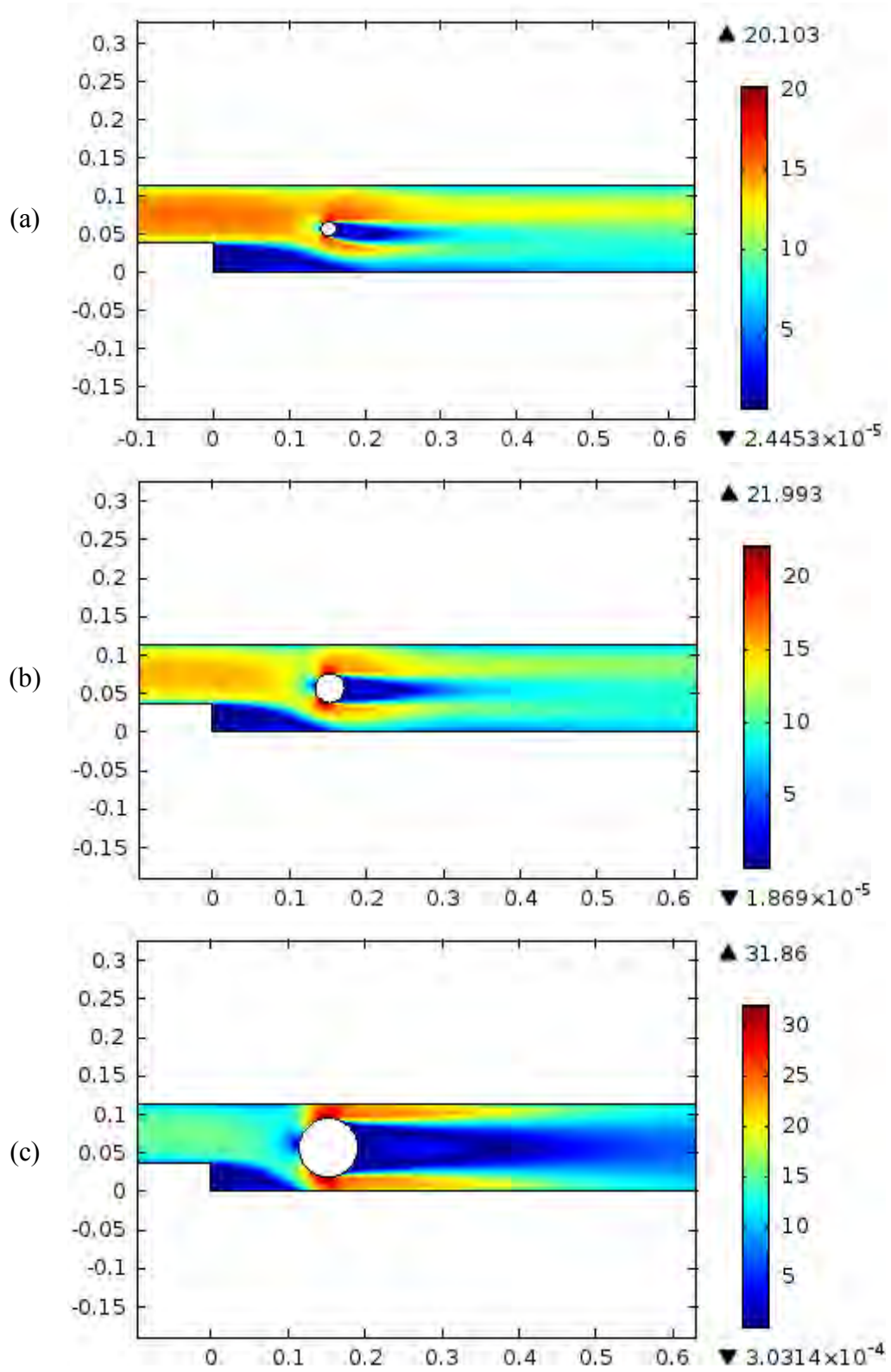
Velocity profiles in Figures 4.5 and 4.6 show the variation at different positions for different sizes of the obstacle. Figures 4.4 and 4.5 display the velocity profile at the cross section at the center of the obstacle and at the downstream at distance  $x = 8H$  respectively. In Figure 4.5 the gaps in the profiles are due to the presence of the solid obstacle. Since the pressure increases with the size of the obstacle the fluid comes out at high speed and reaches more than double of the inlet velocity for the largest one. The lower parts of the profiles project a lesser speed of fluid because of the step present at the lower part of the upstream.

The profiles representing the turbulent kinetic energy  $k$  in the Figures 4.6 and 4.7 show synchronized effect with the velocity profiles and stream lines. From Figure 4.6(c) it is observed that the turbulent kinetic energy  $k$  fluctuates near the obstacle wall at the top and bottom side for the largest obstacle. At the downstream in Figure 4.6 it is seen that for the obstacle sizes  $r = H/4$  and  $r = H/2$  the pattern is almost similar whereas the change is visible for the largest size of the obstacle.

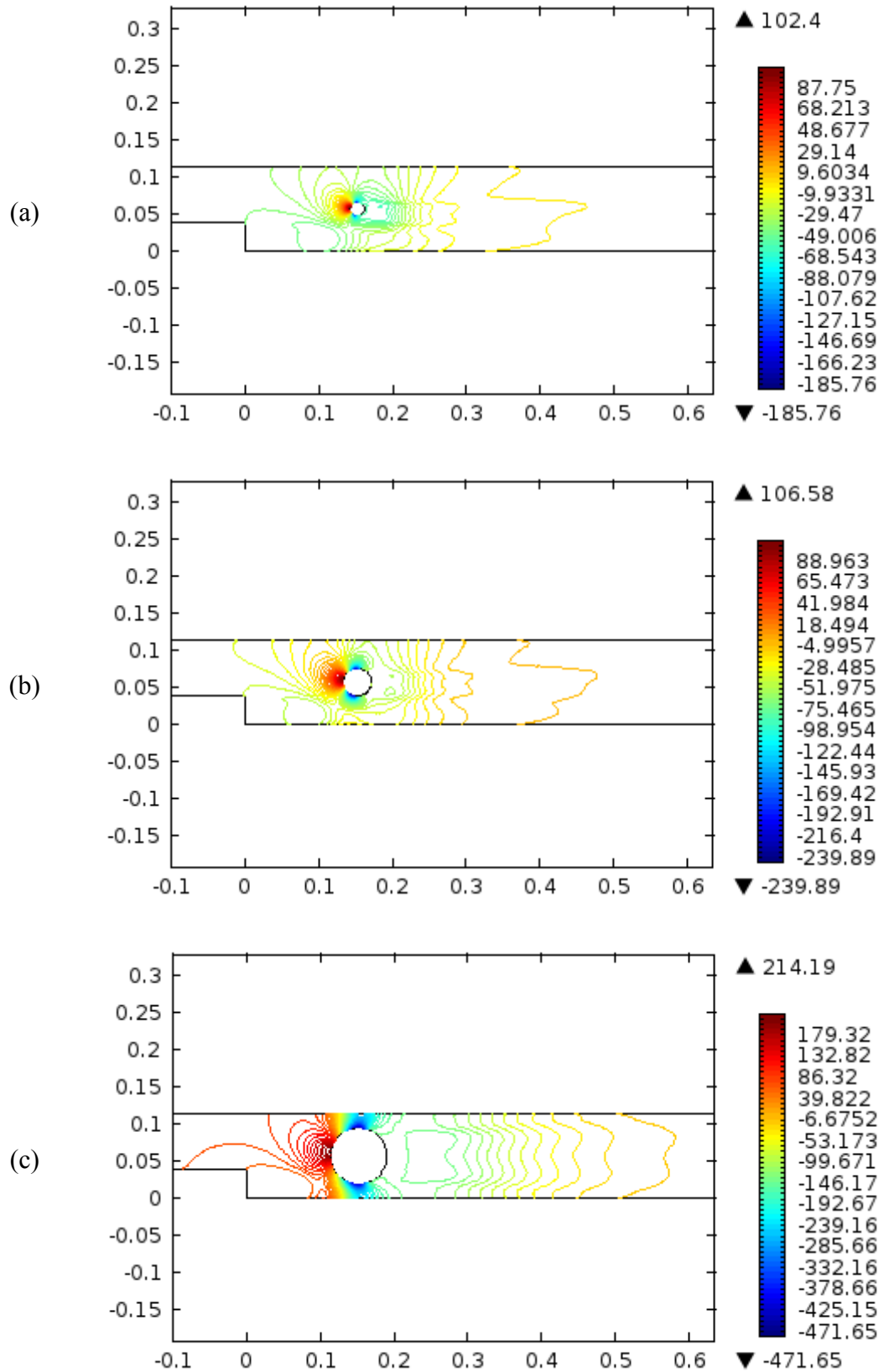
Turbulent dissipation rate  $\varepsilon$  profiles are shown in the Figures 4.9 and 4.10. These profiles are also taken for three obstacle sizes mentioned above. The graph shown in the Figure 4.9 is taken at the center of the obstacle. At the boundary of the obstacle the dissipation values varies sharply. The smaller size of the obstacle shows little dissipation rate values whereas the larger obstacle size shows larger values at the downstream in the Figure 4.10. Also at the downstream it is noticeable that the lower half and the upper half of the profile is not symmetric whilst the larger obstacle size makes the profile sufficiently symmetric as well as increasing the magnitude.



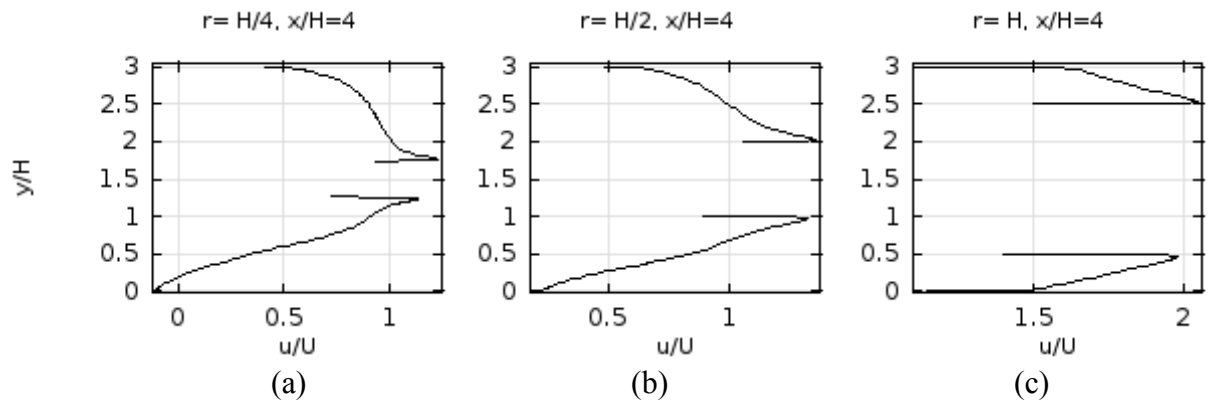
**Figure 4.2:** Stream lines for the different sizes of the circular obstacle: (a) obstacle with radius  $r = H/4$ , (b) obstacle with radius  $r = H/2$  and (c) obstacle with radius  $r = H$ .



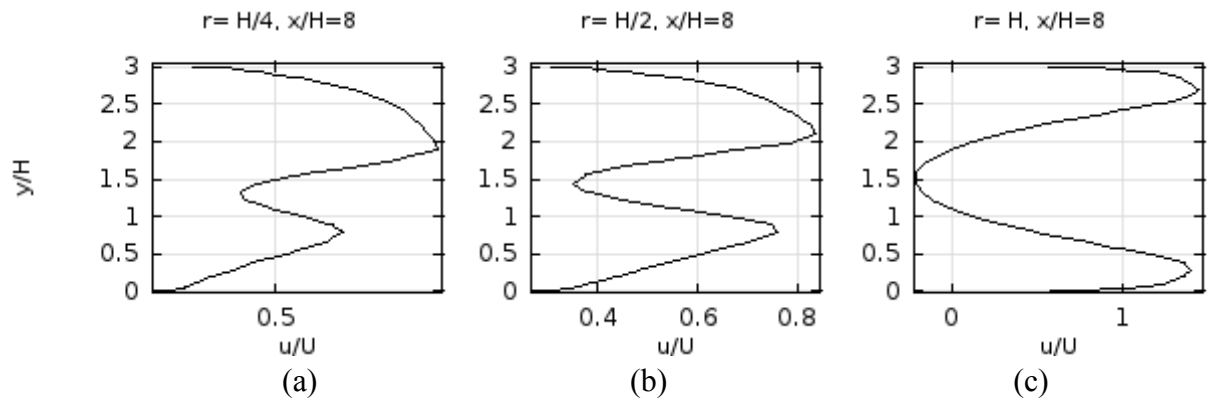
**Figure 4.3:** Velocity magnitude for obstacle size with radius  $r = H/4, H/2, H$ .



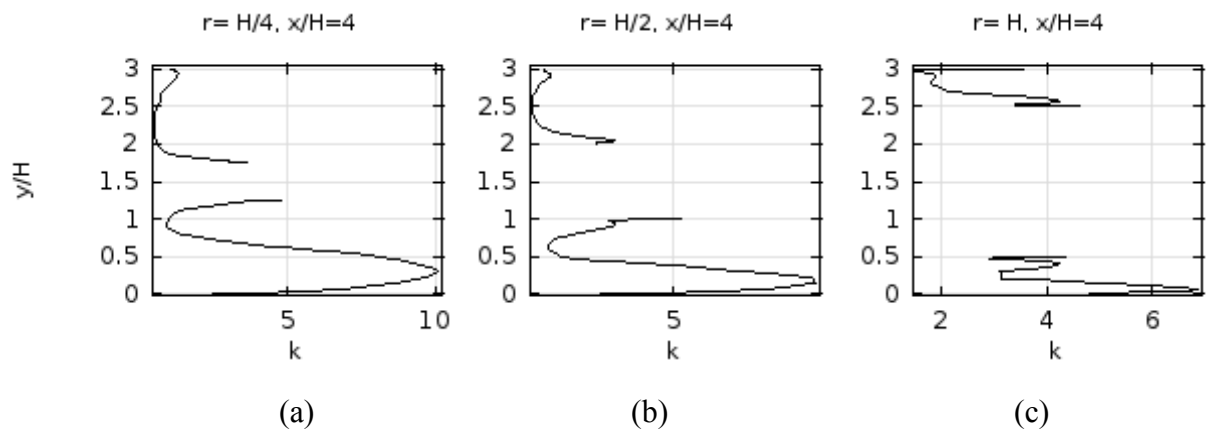
**Figure 4.4:** Pressure distribution for obstacle size with radius  $r = H/4, H/2, H$ .



**Figure 4.5:** Velocity profiles for three obstacle sizes at the center of the obstacle: (a) obstacle with radius  $r = H/4$ , (b) obstacle with radius  $r = H/2$  and (c) obstacle with radius  $r = H$ .

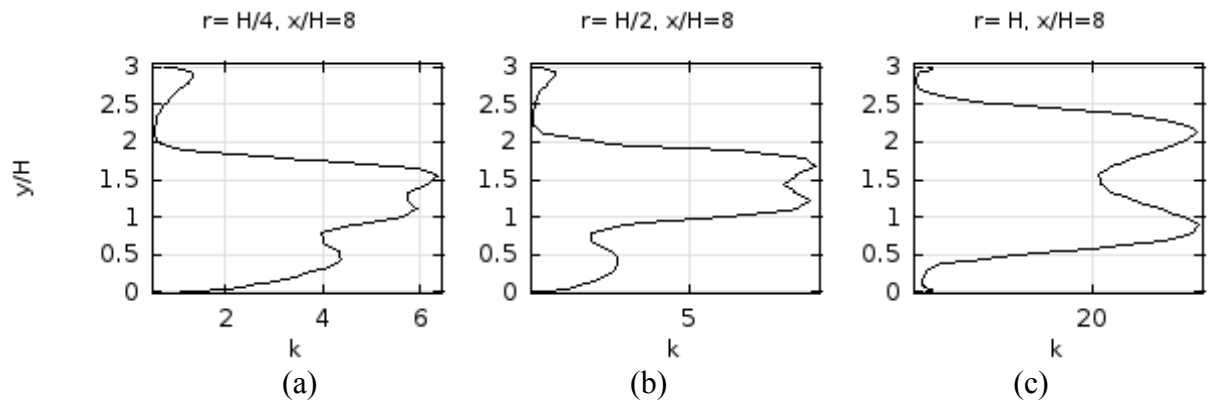


**Figure 4.6:** Velocity profiles for three obstacle sizes at the downstream ( $x/H = 8$ ): (a) obstacle with radius  $r = H/4$ , (b) obstacle with radius  $r = H/2$  and (c) obstacle with radius  $r = H$ .

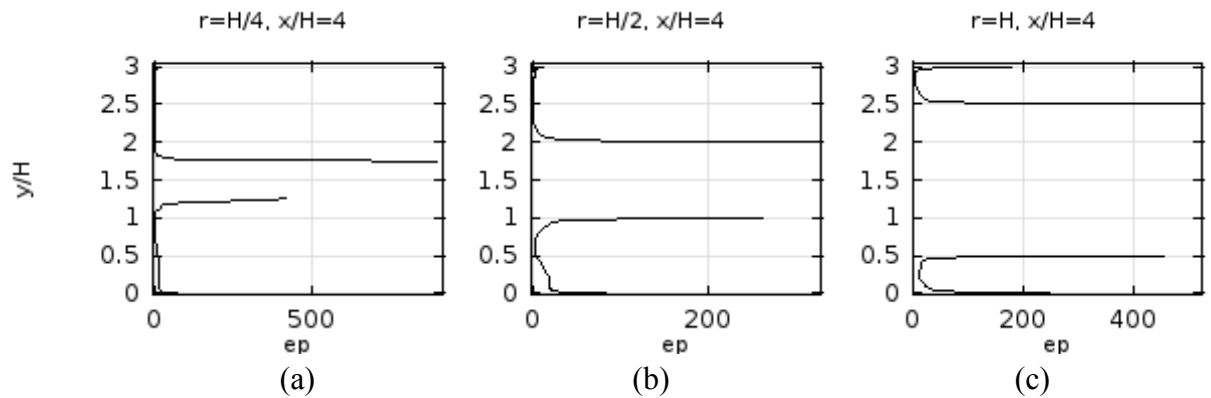


**Figure 4.7:** Turbulent kinetic energy for three obstacle sizes at the center of the obstacle: (a) obstacle with radius  $r = H/4$ , (b) obstacle with radius  $r = H/2$  and (c) obstacle with radius  $r = H$ .

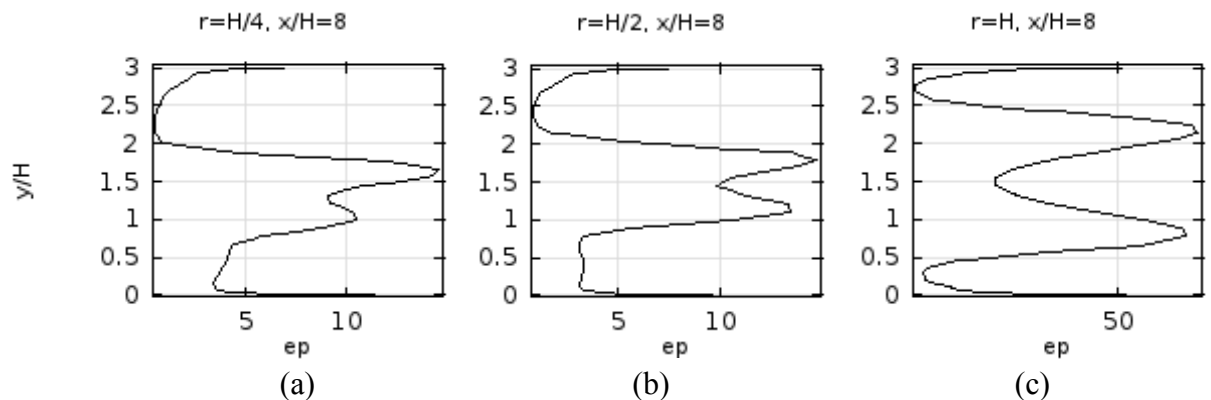




**Figure 4.8:** Turbulent kinetic energy for three obstacle sizes at the downstream ( $x/H = 8$ ): (a) obstacle with radius  $r = H/4$ , (b) obstacle with radius  $r = H/2$  and (c) obstacle with radius  $r = H$ .



**Figure 4.9:** Turbulent dissipation rate for three obstacle sizes at the center of the obstacle: (a) obstacle with radius  $r = H/4$ , (b) obstacle with radius  $r = H/2$  and (c) obstacle with radius  $r = H$ .



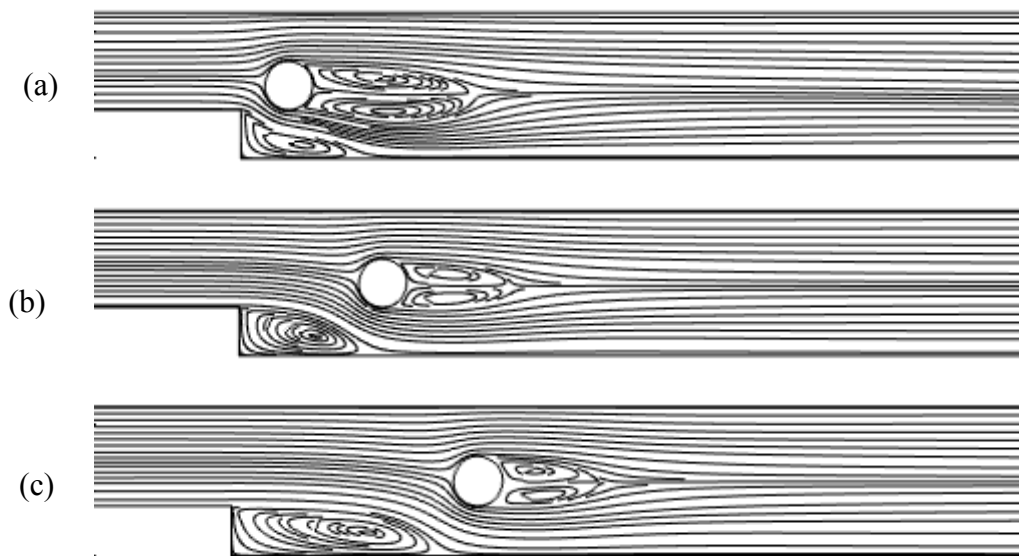
**Figure 4.10:** Turbulent dissipation rate for three obstacle sizes at the downstream ( $x/H = 8$ ): (a) obstacle with radius  $r = H/4$ , (b) obstacle with radius  $r = H/2$  and (c) obstacle with radius  $r = H$ .

## ***4.2 Variation of the Position of the Obstacle***

In this section the position of the circular obstacle is varied keeping its size fixed. The size is kept at  $r = H/2$  and the positions are taken at a distance  $H$ ,  $3H$  and  $5H$  from the step respectively.

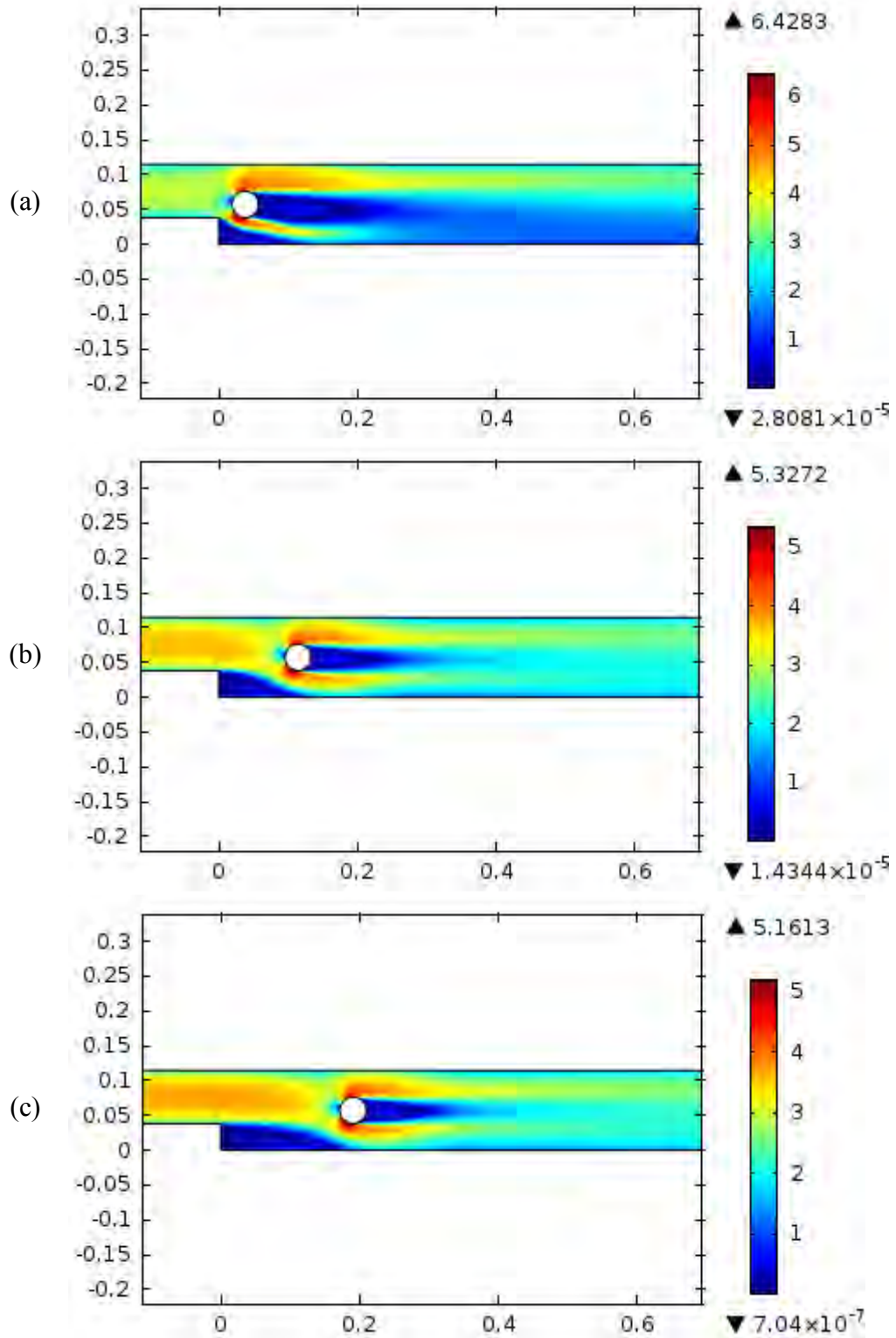
The Figure 4.11 shows the streamlines with the circular obstacle placed at different distances from the step. It is clear from the graphs that the vortices are bigger when the obstacle is nearest to the step. Also it makes the vortex at the step much smaller. This is due to the fact that smaller amount of fluid can enter in that lower region at a certain time. The velocity magnitudes are presented in the Figure 4.12. The lower part of the flow field cannot recover from the low velocities for the closest obstacle to the step due to the same reason stated above. Pressure contours shown in the Figure 4.13 have a similar pattern except the fact that for the nearest obstacle to the step the maximum value is higher than other two cases.

The velocity profiles are shown in the Figure 4.14 for different positions of the obstacle from the step. These profiles are taken at the center of the obstacle. It is observed that at the upper end and the lower end of the obstacle the velocity is much higher for all three cases. The lower part of the profile has smaller magnitude due to the presence of the step upstream. Similar pattern can be seen in the velocity profiles downstream of the obstacle in the Figure 4.15.

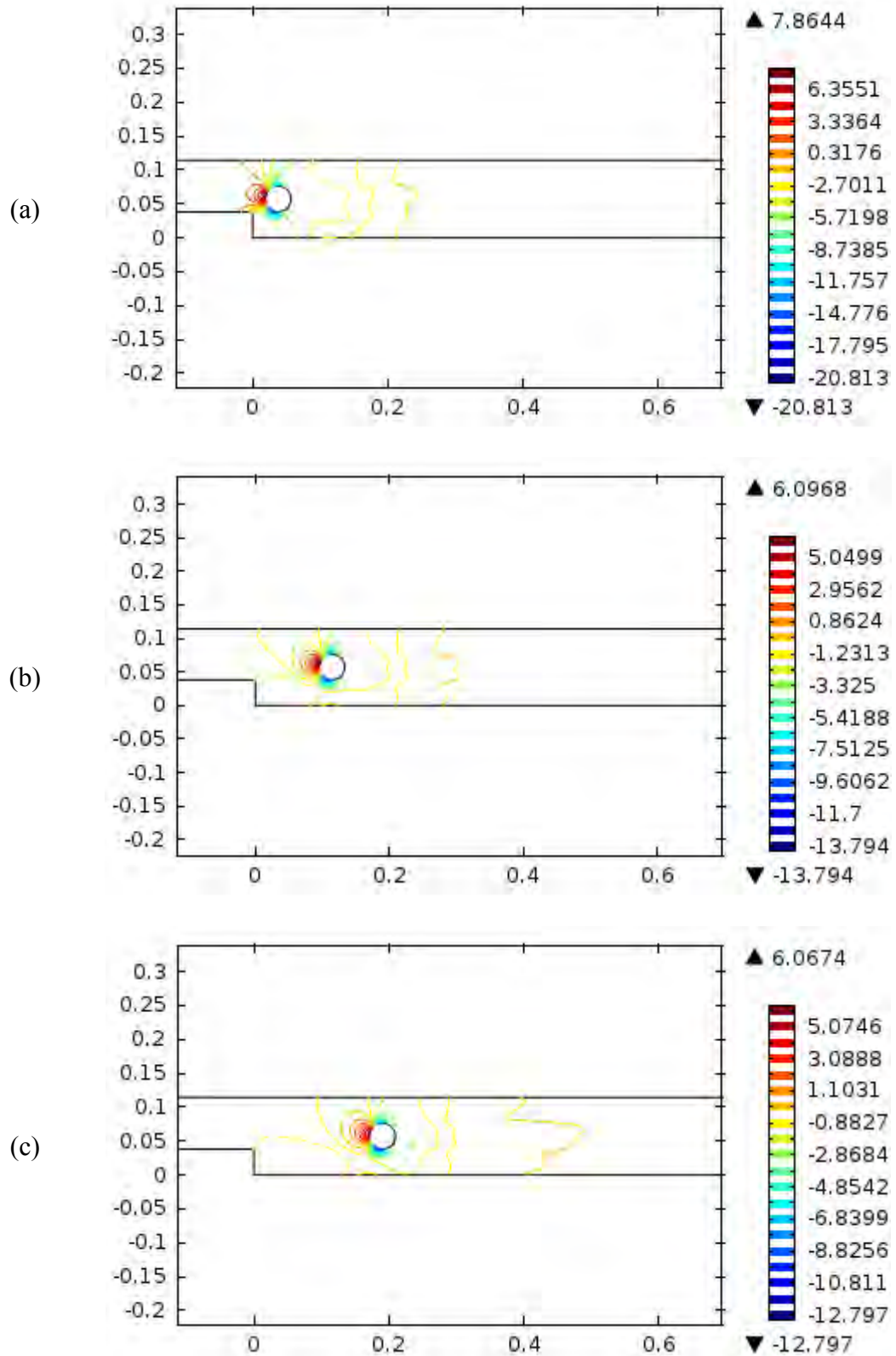


**Figure 4.11:** Stream lines for the different positions of the circular obstacle with size  $r = H/2$ : (a) obstacle with center at distance  $H$  from step, (b) obstacle with center at distance  $3H$  from step and (c) obstacle with center at distance  $5H$  from step.

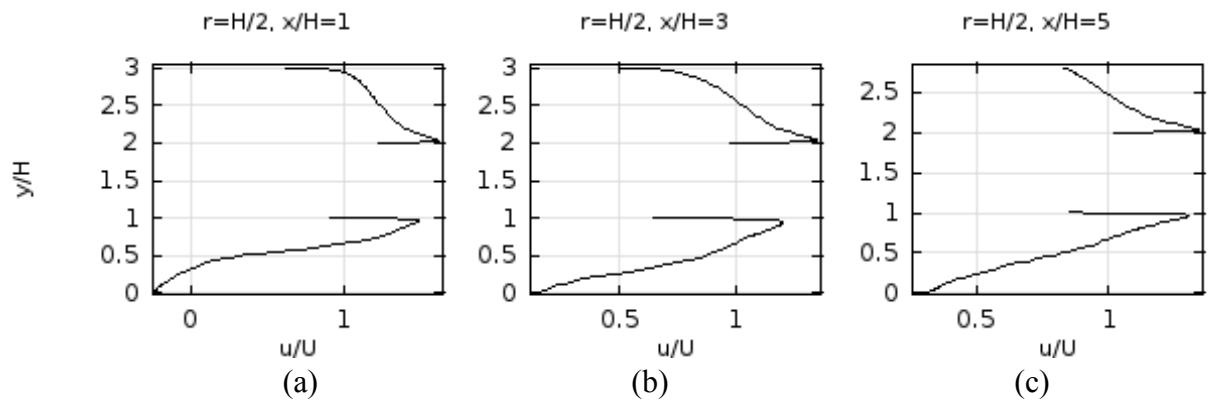
The turbulent kinetic energy profiles are presented in the Figures 4.16 and 4.17. The variations in the lower part are due to the presence of the step at the upstream and are more visible for the obstacle nearest to the step. The turbulent dissipation rate profiles are shown in the Figures 4.18 and 4.19. The higher values in the Figure 4.18 at the lower end of the profiles might be due to the limitations of the model at the boundary. The profiles at the downstream in the Figure 4.19 show lesser and lesser effects of the step on the flow field which is likely as usual.



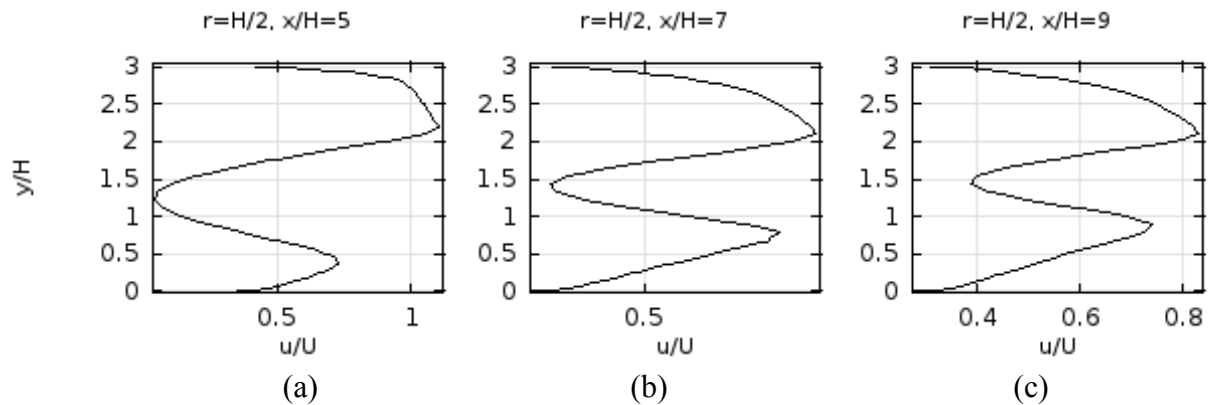
**Figure 4.12:** Velocity magnitude for the different positions of the circular obstacle with size  $r = H/2$ : (a) obstacle with center at distance  $H$  from step, (b) obstacle with center at distance  $3H$  from step and (c) obstacle with center at distance  $5H$  from step.



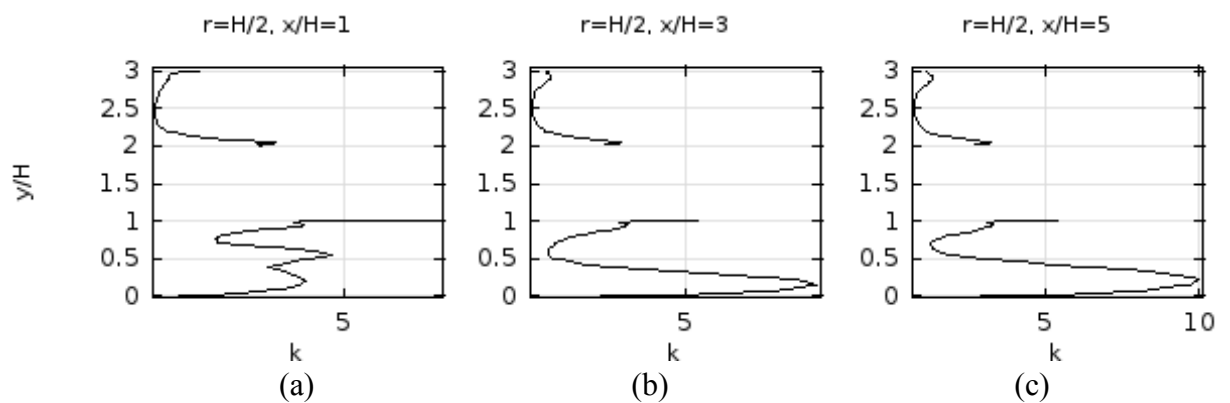
**Figure 4.13:** Pressure distribution for obstacle positions with radius  $H/2$  at: (a) obstacle with center at distance  $H$  from step, (b) obstacle with center at distance  $3H$  from step and (c) obstacle with center at distance  $5H$  from step.



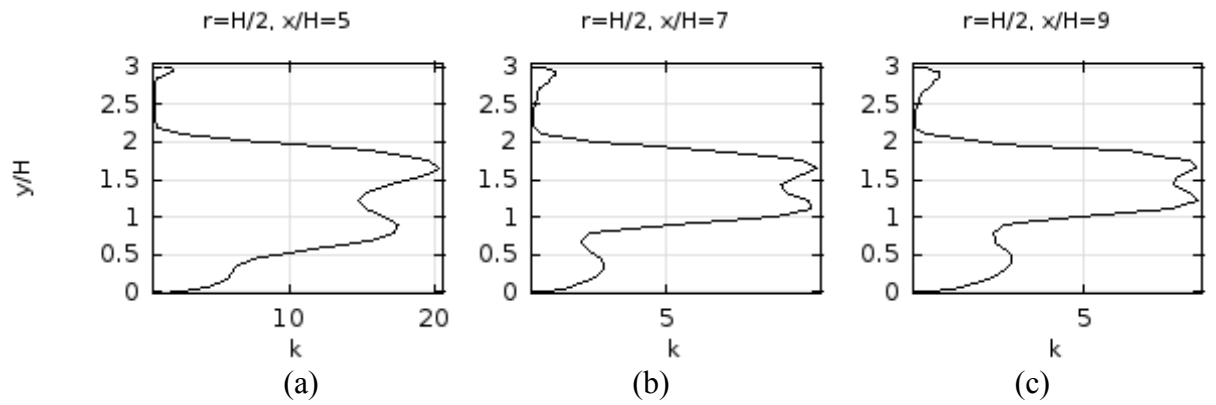
**Figure 4.14:** Velocity profiles for three obstacle positions at the center of the obstacle: (a) obstacle at position  $x/H = 1$ , (b) obstacle at position  $x/H = 3$  and (c) obstacle at position  $x/H = 5$ .



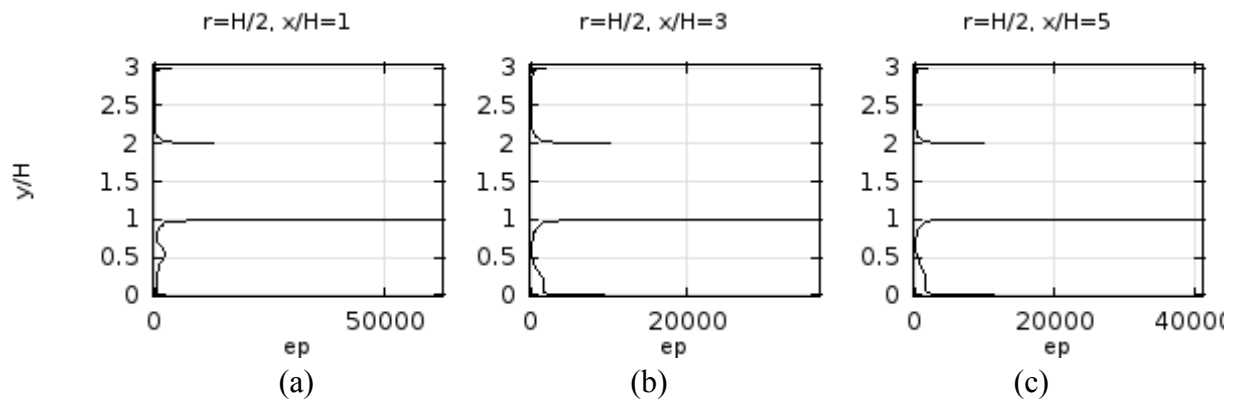
**Figure 4.15:** Velocity profiles for three obstacle positions at the downstream ( $4H$  from the obstacle): (a) obstacle at position  $x/H = 1$ , (b) obstacle at position  $x/H = 3$  and (c) obstacle at position  $x/H = 5$ .



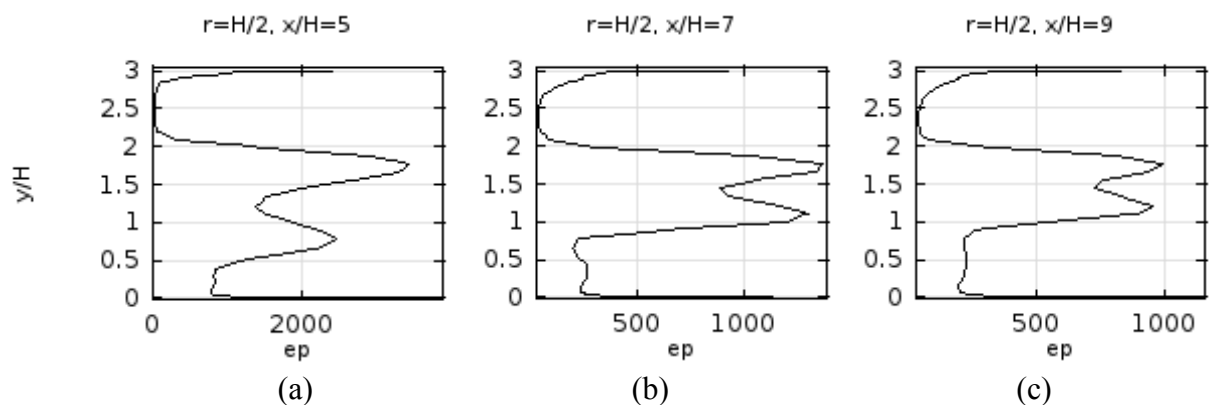
**Figure 4.16:** Turbulent kinetic energy for three obstacle positions at the center of the obstacle: (a) obstacle at position  $x/H = 1$ , (b) obstacle at position  $x/H = 3$  and (c) obstacle at position  $x/H = 5$ .



**Figure 4.17:** Turbulent kinetic energy for three obstacle positions at the downstream ( $4H$  from the obstacle): (a) obstacle at position  $x/H = 1$ , (b) obstacle at position  $x/H = 3$  and (c) obstacle at position  $x/H = 5$ .



**Figure 4.18:** Turbulent dissipation rate for three obstacle positions at the center of the obstacle: (a) obstacle at position  $x/H = 1$ , (b) obstacle at position  $x/H = 3$  and (c) obstacle at position  $x/H = 5$ .



**Figure 4.19:** Turbulent dissipation rate for three obstacle positions at the downstream ( $4H$  from the obstacle): (a) obstacle at position  $x/H = 1$ , (b) obstacle at position  $x/H = 3$  and (c) obstacle at position  $x/H = 5$ .

# Chapter 5

## Conclusion

### *5.1 Conclusions from the Present Study*

Two situations were considered in the above study namely the variations of the size of the obstacle and the variations of the positions of the obstacle in the backward facing step flow field. Standard  $k-\varepsilon$  turbulence model was used to describe the turbulent flow. The model was solved using the finite element method and the results are presented graphically in terms of streamlines, velocity magnitude, pressure, velocity profiles, turbulent kinetic energy and turbulent dissipation rate profiles etc. The following conclusions can be derived from the above numerical investigations:

- The obstacle size and position changes the flow and energy configurations significantly.
- The flow remains turbulent up to a considerable distance from the obstacle and the turbulence grows higher when the step and the obstacle are nearer.
- Velocity reaches as high as double from the initial one for largest obstacle size in the narrower part of the flow field.
- The leading face of the obstacle encounters high pressure and grows with the size of the obstacle.
- Highest turbulent kinetic energy fluctuation in the flow field between channel and the top end and the bottom end of the obstacle is observed for the largest obstacle.



## ***5.2 Suggestions for Further Study***

For further study on this topic several suggestions can be made. First of all in the present study the standard  $k-\varepsilon$  turbulence model was used. Other turbulence models based on RANS equations can be used on this geometry. These models can include but not limited to low Reynolds number  $k-\varepsilon$  turbulence model,  $k-\omega$  turbulence model, RNG turbulence model, Spalart-Allmaras turbulence model etc. Also models based on the large eddy simulation technique and direct numerical simulation technique can be used provided that sufficient computing power is available.

On the other hand the geometry can be modified further by taking different types of obstacles in the flow field. These can include square, rectangle, an airfoil, other designs of vessels etc.

## References

- Abe, K., T. Kondoh, and Y. Nagano, A New Turbulence Model for Predicting Fluid Flow and Heat Transfer in Separating and Reattaching Flows—I. Flow field calculations, *International Journal of Heat and Mass Transfer*, vol. 37, no. 1: 139–151, 1994.
- Boussinesq, J., “Theorie de l’Ecoulement Tourbillant,” *Mem. Presents par Divers Savants Acad. Sci. Inst. Fr. Vol. 23*, pp. 46-50, 1877.
- Bradshaw, P. “The Understanding and Prediction of Turbulent Flow,” *The Aeronautical Journal*, Vol. 76, No. 739, pp. 403-418, 1972.
- Cebeci, T. and Smith, A. M. O., *Analysis of Turbulent Boundary Layer*, Ser. in appl. Math. & Mech., Vol XV, Academic Press, Orlando, FL., 1974.
- Chou, P. Y., “On the Velocity Correlations and the Solution of the Equations of Turbulent Fluctuation,” *Quart. Appl. Math.*, Vol. 3, pp. 38, 1945.
- Codina, R. and O. Soto, “Finite element Implementation of Two-equation and algebraic stress turbulence Models for Steady Incompressible Flows”, *Int. J. Numer. Meth. in Fluids*, Vol. 30, pp. 309-334, 1999.
- Driver, D. M., and H. L. Seegmiller, Features of a Reattaching Turbulent Shear Layer in a Divergent Channel Flow, *AIAA J. Vol. 23 No. 2*, pp. 163-171, 1985.
- Hinz, J. O., *Turbulence*, Second Ed. McGraw Hill, New York, NY, 1975.
- Holman, J. P. *Heat Transfer*. McGraw-Hill, p. 207, 2002.

Ilinca, F., and D. Pelletier, "Positivity Preservation and Adaptive Solution for the  $k-\varepsilon$  Model of Turbulence", 35<sup>th</sup> Aerospace Sciences Meeting & Exhibit, Reno, USA, AIAA Journal, Vol. 97, No. 0205, 1997A.

Ilinca, F., D. Pelletier and F. Arnoux-Guisse, "An Adaptive finite Element Scheme for Turbulent Free Shear Flows", Int. J. Comp. Fluid Dyn., Vol. 8, pp. 171-188, 1997B.

Jehad, D. G., G. A. Hashim, A. K. Zazoor, C. S. N. Azwardi, Numerical Study of Turbulent Flow over Backward Facing Step with Different Turbulence Models, J. Adv. Res. Des. vol 4, no. 1: 20-27, 2015.

Kim, J., Investigation of Separation and Reattachment of Turbulent Shear Layer: Flow over a Backward Facing Step, PhD. Thesis, Stanford University, 1978.

Kolmogorov, A. N., "Equations of Turbulent Motion of an Incompressible Fluid," Izvestia Academy Of Sciences, USSR; Physics, Vol. 6, Nos. 1 and 2, pp. 56-58, 1942.

Kuzmin, D., O. Mierka, and S. Turek, On the Implementation of the  $k-\varepsilon$  Turbulence Model in Incompressible Flow Solvers Based on a Finite Element Discretization, International Journal of Computing Science and Mathematics, vol. 1, no. 2-4, pp. 193-206, 2007.

Lasher, William C., Dale B. Taulbee, On the Computation of Turbulent Backstep Flow, International Journal of Heat and Fluid Flow, Volume 13, Issue 1: 30-40, March 1992.

Launder, B.E., Spalding, D.B., The numerical computation of turbulent flows, Computer Methods in Applied Mechanics and Engineering, Vol. 3, No. 2, pp. 269-289, 1974.

Lew, A. J., G. C. Buscaliga and P. M. Carrica, A Note on the Numerical Treatment of the k-epsilon Turbulence Model. Int. J. of Comp. Fluid Dyn. Vol. 14, pp. 201-209, 2001.

Prandtl, L., "Über die ausgebildete Turbulenz," ZAMM, Vol. 5, pp. 136-139, 1925.

Prandtl, L., "Über ein neues Formelsystem für die ausgebildete Turbulenz," Nachr. Akad. Wiss. Göttingen, Math-Phys. Kl., pp. 6-19, 1945.

Ratha, D., A. Sarkar, Analysis of Flow over Backward Facing Step with Transition, J. Front. Struct. Civ. Eng. vol 9(1), pp. 71-81, 2015.

Reynolds, O. "On the Dynamical Theory of Incompressible Viscous Fluids and the Determination of the Criterion," Philosophical Transactions of the Royal Society of London. Series A, Vol. 186, P. 123, 1895.

Rotta, J. C., "Statistische Theorie nichthomogener Turbulenz," Zeitschrift für Physik, Vol. 129, pp. 547-572, 1951.

Tennekes, H. and Lumley, J. L., A First Course in Turbulence, MIT Press, Cambridge, MA., 1983.

Utnes, T., "Two Equations ( $k, \epsilon$ ) Turbulence Computations by the Use of a Finite Element Model", Int. J. Numer. Meth. in Fluids, Vol. 8, pp. 965-975, 1988.

von Karman, T. "Turbulence", Twenty Fifth Wilbur Wright Memorial Lecture, Journal of the Aeronautical Sciences, Vol. 41, 1109, 1937.

von Karman, T., –Mechanische Ähnlichkeit und Turbulenz,” Proc. Int. Congr. Appl. Mech., 3<sup>rd</sup>, Stockholm, Part 1, pp. 85-105, 1930.

Wilcox, D.C., Turbulence Modeling for CFD, 3rd ed., DCW Industries, 2006.